Electrochemical Oxidation of Methane to Methanol on Electrodeposited Transition Metal Oxides

Kangze Shen,† Simran Kumari,† Yu-Chao Huang, Joonbaek Jang, Philippe Sautet and Carlos G. Morales-Guio*.

Department of Chemical and Biomolecular Engineering, University of California, Los Angeles, CA 90095, United States.

KEYWORDS. Methane, C-H Activation, Methane Partial Oxidation, Electrocatalysis, Energy, Chemicals.

ABSTRACT: Electrochemical partial oxidation of methane to methanol is a promising approach to the transformation of stranded methane resources into a high-value, easy-to-transport fuel or chemical. Transition metal oxides are potential electrocatalysts for this transformation. However, a comprehensive and systematic study of the dependence of methane activation rates and methanol selectivity on catalyst morphology and experimental operating parameters has not been realized. Here we describe an electrochemical method for the deposition of a family of thin-film transition metal (oxy)hydroxides as catalysts for the partial oxidation of methane. CoO_x, NiO_x, MnO_x and CuO_x are discovered to be active for the partial oxidation of methane to methanol. Taking CoO_x as a prototypical methane partial oxidation electrocatalyst, we systematically study the dependence of activity and methanol selectivity on catalyst film thickness, overpotential, temperature and electrochemical cell hydrodynamics. Optimal conditions of low catalyst film thickness, intermediate overpotentials, intermediate temperatures, and fast methanol transport are identified to favor methanol selectivity. Through a combination of control experiments and DFT calculations, we show that the oxidized form of the as-deposited (oxy)hydroxide catalyst films are active for the thermal oxidation of methane to methanol even without the application of a bias potential, demonstrating that high valence transition metal oxides are intrinsically active for the activation and oxidation of methane to methanol at ambient temperatures. Calculations uncover that electrocatalytic oxidation enables to reach an optimum potential window in which methane activation forming methanol and methanol desorption are both thermodynamically favorable, methanol desorption being favored by competitive adsorption with hydroxide anion.

INTRODUCTION

The direct partial oxidation of methane to methanol is one of the grand challenges in the area of catalysis and energy.[1] Methane is the major constituent of associated petroleum gas which is routinely flared at remote oil fields where its collection and use are unprofitable. The energy losses associated with flaring are roughly equivalent to the natural gas demand of Central and South America resulting in significant economic losses, while the associated greenhouse gas (GHG) emissions result in adverse effects on the climate and environment.[2, 3] In 2021 alone, gas flaring was responsible for the emission of 361 million metric tons (MMT) of CO_2, 39 MMT of CO_2 equivalent in non-combusted methane, and other GHGs and pollutants. There are large environmental and economic incentives to develop technologies for the decentralized transformation of methane into easy-to-transport liquid methanol as these would reduce GHG emissions,[1, 4] increase global carbon utilization, and expand the global methanol production capacity. Methanol current annual global demand is close to 100 MMT and is further projected to rise at a compound annual growth rate of over 5% to double by 2030.[5] This increase in methanol demand is primarily due to expansion of consumption by the automotive and olefin industries. Therefore, new and efficient technologies for the production of methanol from methane at medium and small scales[6] could offer a paradigm shift by connecting directly stranded carbon and energy resources to the base chemicals and energy markets.

The direct transformation of methane to methanol in remote locations requires selective catalysts capable of operating at near-ambient temperatures inside a modular device.[7-11] Although various catalytic systems have been studied for more than 100 years,[12-15] these have never reached commercialization due to low yields and poor selectivity. The main challenge in developing a selective and efficient catalyst for the direct partial oxidation of methane to methanol originates from the difficulty to simultaneously control the kinetics for i) the regeneration of the catalytic active site, ii) the transport, activation and hydroxylation of methane, and iii) the desorption and removal of the produced methanol (Figure 1). Traditional catalytic systems require high temperatures or use strong oxidizing agents to regenerate the catalytic site and overcome the barrier for methane C-H bond activation. Under these reaction conditions, it is difficult to prevent overoxidation of methanol to CO and CO_2. Particularly, the oxygen atom in the produced methanol binds strongly to the metal site and re-

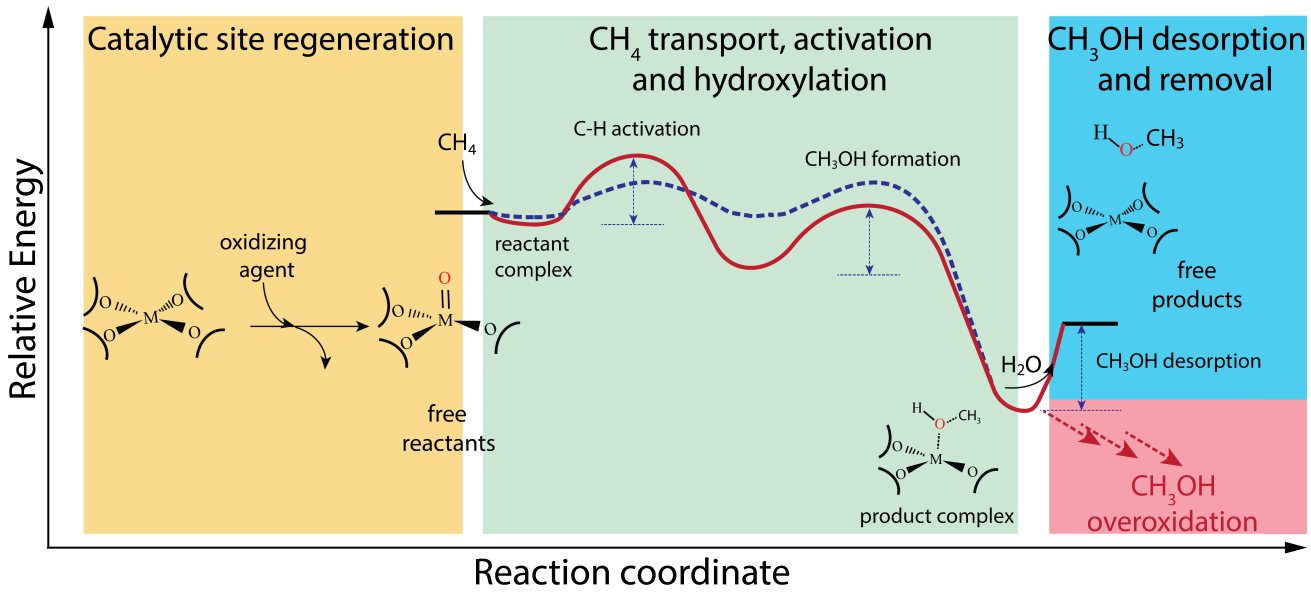

Figure 1. Schematic representation of the most important steps in direct methane to methanol oxidation. The simplified reaction energy diagram includes: the regeneration of the active site by an oxidizing agent or electron collector, the activation and hydroxylation of methane through two hypothetic reaction pathways (ionic in red trace and radical in blue trace), and the endothermic solvent-assisted desorption of methanol along the competing methanol overoxidation. Parasitic decomposition of the regenerated catalytic site and non-catalytic oxidation of methanol are not shown for simplicity.

quires the use of a solvent (i.e. H_2O in Figure 1) to desorb methanol and stabilize the reduced catalyst center.[16] Slow methanol desorption makes the product complex prone to overoxidation and introduces additional layers of complexity.[17, 18] Because of the multiple steps that need to be simultaneously controlled during the direct transformation of methane to methanol, developing selective and efficient catalysts[19] for this transformation has become one of the most remarkable challenges in synthetic catalysis.

Enzymatic systems, on the other hand, offer clues on how to selectively catalyze this transformation. Methane monooxygenase, for example, catalyzes the transformation of methane directly to methanol with exceptional selectivity under ambient conditions. This is achieved through the exquisite control on the transport of oxygen, methane, protons and electrons to the transition iron(IV)-oxo complex in the active center.[17, 20] Conformational changes prevent consecutive oxidation and back diffusion and are responsible for the isolation of the active site and the exceptionally high selectivity for methanol.[21]

Electrocatalysis offers a precise control over the surface oxidative power via the applied potential and is a promising approach to control kinetics and impart product selectivity in the oxidation of methane to methanol just as in the enzymatic system.[1] Electrocatalysts can also replicate many of the mechanistic features in methane monooxygenases through the rational design and control of the electrostatic interactions between catalytic sites on the electrode surface, and the reactants and products penetrating the relatively immobile solvated ions that make up the coordination environment at the electric double layer. Advanced methane to methanol electrocatalyst should i) bring methane into the active site in the appropriate orientation to lower activation energy barriers and accelerate the rates of transformation, ii) regenerate metal-oxo species on electrode surfaces directly from water and remove electrons at slow rates relative to methanol desorption and overoxidation, and iii) have an electrode architecture with a high density of active sites connected to fast methanol transport and collection networks.

Over the last decade, the use of transition metal oxides as catalyst for the electrochemical partial oxidation of methane to methanol has drawn significant interest. Mustain and co-workers, for example, have shown that binary transition metal oxides of NiO/ZrO_2 catalyze the electrochemical oxidation of methane in carbonate electrolytes.[22-24] Park and co-workers also utilized a chemical precipitation method to prepare Co_3O_4/ZrO_2 nanocomposites and Co_3O_4 powder/ZrO_2 nanotubes that show activity for the production of higher alcohols such as 1-propanol and 2-propanol.[25, 26] In these works, the introduction of zirconia to unary transition metal oxides has been suggested to be indispensable in order to promote methane partial oxidation in the presence of the carbonate ions. The challenge in these works utilizing particle catalysts is, however, that zirconia has multiple additional effects on transport which are poorly understood and must be deconvoluted. For example, the introduction of the catalytically inert, non-conductive zirconium oxide leads to different catalyst morphologies and spatial distributions of the active phase of the catalyst. These differences should be expected to affect selectivity as these modify the residence time of the methanol intermediate near the oxide surface and thus modify the probability for methanol overoxidation.[27] The requirement to use carbonate as mild oxidant is also not fully understood. Porous hollow fiber NiO/Ni anodes and iron-nickel hydroxide nanosheets have also been reported to

produce methanol and ethanol as methane electrochemical oxidation products in aqueous hydroxide solutions where carbonate is not present in significant amounts.[28-30] CO_2 generated by the overoxidation of methane is likely to react with the highly alkaline environment to form carbonate in solution, but whether this carbonate can in turn become the major oxidant is not clear. It must also be noted that the faradaic efficiencies (FEs) in some of these systems exceed 100% (Table S1) implying that chemical reactions between methane and stoichiometric oxidants in the oxide catalyst or the electrolyte contribute to methane oxidation and could be responsible in part for the production of oxygenates. The production of methanol and other carbon products could also be the result of the degradation of carbon conductive materials and binders added in the preparation of the catalyst inks in some of these systems. To date, the intrinsic mechanisms for the activation of methane and the formation of methanol are largely unknown and are likely obscured by the lack of consistency across the existing literature with regards to the electrochemical setups used, the morphology of the catalysts, the composition of the electrolytes, the analytical tools used for product quantification, as well as the standards used for the reporting of activity, selectivity, and faradaic efficiency.

Recently, Prajapati *et al*. demonstrated a comprehensive work that avoids the use of carbon conductive materials or binders and utilizes the surface oxides formed on metals upon electrochemical oxidation to show that four types of different transition metal oxides (TiO_2, IrO_2, PbO_2, and PtO_2) are active for the electrochemical methane oxidation reaction to CO_2 at oxidative potentials positive of 1.1 V vs SHE. A bimetallic Cu_2O_3 on TiO_2 catalyst was reported, where Cu was proposed to modify the reaction barrier for the key intermediates and facilitate the desorption of CH_3OH showing faradaic efficiencies for methanol of up to 6%.[31] Although these electrocatalysts have been shown to activate methane, none of the unary metal oxides was reported to produce methanol. Potential-dependent theoretical studies have suggested that methane oxidation on oxidized transition metal surfaces proceeds favorably at oxidative potentials where oxygen evolution also occurs.[31-33] The mechanism for the formation of methanol and the factors controlling its selectivity, however, are not well understood.

In order to gain a better understanding of the underlying mechanisms for methane partial oxidation, we have systematically approached this reaction through the breakdown of the three competing rates in the oxidation of methane to methanol (Figure 1), namely, we have attempted to determine to the best of our abilities i) the rate of catalytic site regeneration and oxygen evolution; ii) the rate of methane transport, activation and hydroxylation; and iii) the rate of desorption and removal of the produced methanol. We have done this through the combination of high sensitivity product quantification tools, the use of advanced electrochemical reactors with well-characterized transport properties, and the design of experiments tailored to systematically decouple the multiple convoluted steps summarized in Figure 1. These experiments are combined to first-principle atomistic simulations to provide mechanistic understanding.

As a first step, we have decided to circumvent the use of catalyst inks. Here, we have used a one-step electrodeposition method for the preparation of transition metal (oxy)hydroxides as electrocatalysts. The oxidative electrodeposition method utilized here is self-limiting in growth and allows the deposition of largely amorphous, thin-film conductive metal (oxy)hydroxide films of known activity for water oxidation, well-defined charge transport mechanisms and measurable charge transport resistance.[34] Upon testing of these materials, we discover that CoO_x, NiO_x, CuO_x and MnO_x prepared via electrodeposition are active for the methane partial oxidation to methanol. In this work, we show that the detection and quantification of methanol and other oxidation products depends on the electrochemical cells used and the conditions for the collection of liquid and gas samples as reaction-transport kinetics control methanol product selectivity. Through the utilization of an advanced gas-tight cell with a rotating cylinder electrode, unique conditions of hydrodynamics for the partial oxidation of methane are realized, elucidating the importance of the control on both kinetics and mass transfer for each of the steps involved in the reaction. Calculations show an optimum potential window for selective methane oxidation into methanol.

EXPERIMENTAL SECTION

Electrocatalyst materials and preparation. Sodium acetate (NaOAc, anhydrous, ≥99%), Cobalt(II) chloride ($CoCl_2$, anhydrous, >98%) and manganese(II) chloride ($MnCl_2$, tetrahydrate, 97%) were purchased from Sigma-Aldrich. Nickel(II) acetate (NiOAc, tetrahydrate, 98%), iron(II) chloride ($FeCl_2$, tetrahydrate, 99%), and copper(II) acetate ($Cu(CH_3COO)_2$, anhydrous, 99%) were purchased from Fisher Scientific. Millipore deionized water (18.2 MΩ cm) was used to prepare all of the electrodeposition baths. The concentrations of precursors used in electrodepositions of the different catalysts and specific pH are compiled in Table S2. Sodium acetate (0.1 M NaOAc) was used in all of the electrodeposition baths as supporting electrolyte. The pH of the baths was adjusted using either 0.1 M acetic acid solution or 0.1 M sodium hydroxide solution. All of the electrodeposition experiments were carried out under atmospheric conditions unless mentioned otherwise.

Catalyst electrodeposition. An Autolab PGSTAT302N potentiostat/galvanostat was used for electrodeposition of the different transition metal oxides in a three-electrode setup with a titanium cylinder substrate (active geometric area = 3 cm^2) as the working electrode, a graphite foil as the counter electrode, and an Ag/AgCl as the reference electrode. Prior to use, the surface of the titanium cylinder electrode was polished using an alumina slurry suspension of 0.05 μm grain size on a microcloth polishing pad (Buehler), rinsed thoroughly with Millipore deionized water (18.2 MΩ cm), and sonicated in deionized water for 10-15 minutes. Prior to electrodeposition, the titanium cylinder electrode was immersed in 2.5 M hydrochloric acid for 60 minutes to remove surface oxides. The titanium cylinders were then rinsed in deionized water and dried under Ar flow. In the electrodeposition process, all the applied potentials were measured against the Ag/AgCl reference electrode. Except for copper, electrodeposition of all the other catalysts was performed by 5 or 100 cycles of consecutive

linear sweep voltammetry (LSV) within a specific potential window from 0.8 to 1.1 V vs Ag/AgCl at a scan rate of 10 mV s^{-1}. The deposition of most metal oxides was done using oxidative potentials ($M^{2+}(aq) \rightarrow MOOH(s) + e^- + 3H^+$) where the transition metal deposits on the surface of the electrode directly as an (oxy)hydroxide. As the oxidative electrodeposition proceeds, the oxygen evolution rate increases lowering the local pH and leading to the dissolution of the electrodeposited film. To suppress catalyst dissolution, the most positive potential during the LSV deposition was decreased by 50 mV after the 40th and 70th LSV. Copper, on the other hand was deposited under constant applied potential (–0.18 V vs Ag/AgCl) for 5 min via reductive deposition of the catalyst ($2Cu^{2+} + 2e^- + H_2O \rightarrow Cu_2O + 2H^+$). The potential vs current curves for the oxidative electrodeposition experiments and time vs current data for the copper deposition are shown in Figure S1.

Electrochemical rotation cell setup for methane partial oxidation experiments. A gas-tight rotating cylinder electrode (RCE) cell recently reported by us[27, 35] was used for all the methane partial oxidation studies in this work. In the RCE cell, a follower magnet inside the cap traces a driver magnet outside the cell via magnetic coupling that allows for the rigorous control of the mass transport in the cell (Figure 2). The cell's cap carries the electrical connections and is designed to reduce the headspace above the electrolyte in the working electrode compartment. The cap for the working electrode compartment has three threaded ports to accommodate leak-free gas fittings (Swagelok). One of these ports is connected to a glass frit for the feeding of the CH_4 into the working electrode compartment, bringing in the gas feed and bubbling it directly into the electrolyte ensuring a high surface area for contact between the gas and the electrolyte and the consequent saturation of the liquid with dissolved methane. A second port serves as the gas outlet which transfers gaseous products out to the gas chromatogram (GC) connected to the RCE cell for the on-line detection and quantification of gaseous products. The last threaded port is used to draw out liquid aliquots for further quantification of liquid products via nuclear magnetic resonance (NMR). This port is also used to measure the electrolyte temperature at intervals during an experiment. In all experiments involving methane partial oxidation, methane is also bubbled in the counter electrode compartment. This is to keep similar gas environments in both cell compartments thus suppressing dissolved gas crossover. Hex screws that go through the entire lower compartments and nuts are used to compress and seal the cell. A cooling block with a heat-exchange area of 16 cm^2 is positioned below the bottom of the RCE working electrode chamber for temperature control. Liquid products accumulate in the cell over time and thus aliquots are drawn out at intervals of 20 minutes for analysis using a 500 MHz NMR.

Reactor kinetics. In methane partial oxidation experiments, we measure *reactor kinetics* and not *reaction kinetics*. The reactor kinetics in the RCE cell cannot be classified as either being of a batch, semi-batch or flow type. On one hand, a flow type reactor assumes low back mixing so that concentration gradients are a function of position along the flow path and it also assumes that these concentrations are not a function of time. Despite the continuous flow of gas in the RCE cell, liquid products accumulate in the electrolyte while some gas products are stripped away (i.e. O_2) and others of acidic nature such as CO_2 are absorbed in the alkaline electrolyte in the form of carbonates. A batch type reactor, on the other hand, assumes that the concentration is not a function of position but only a function of time. Our reactor system has a 3-dimmensional distribution of reactants, products and charge carriers that fluctuate as a function of time (*vide infra*). Therefore, the reaction kinetics in our reaction system are those of a *gastight rotating cylinder electrode cell* with accumulation of products and intermediates in the liquid phase of the cell. We have recently reported a detailed analysis of the hydrodynamics in these systems and how these affect reactor kinetics in Jang et al.[27] and Richard et al.[35] At the electrode/electrolyte interface, the reactor kinetics are better described by a continuously-stirred tank reactor (CSTR) approximation that captures the accumulation of products and their residence time near the surface of the electrode as well as the high local conversion of methane as external mass transport limits the supply of methane to the surface of the catalyst.

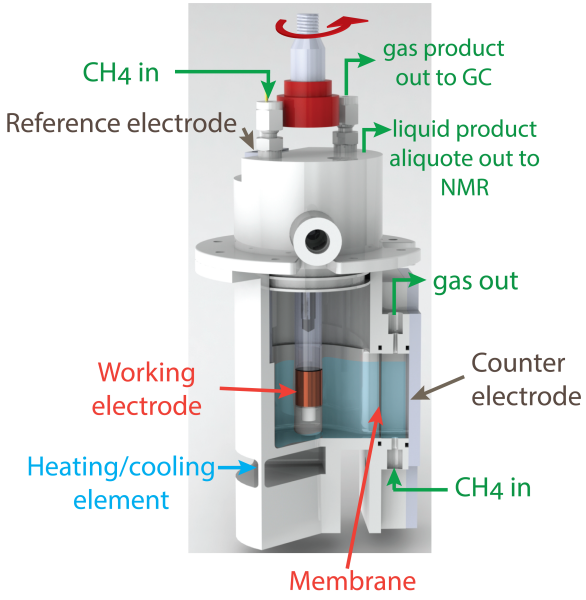

Figure 2. Schematic of the gas-tight electrochemical cell with a rotating cylinder electrode. Adapted with permission.[27] Copyright 2022 Wiley.

Electrochemical measurements. Prior to setting up of the cell, transition metal (oxy)hydroxides were freshly electrodeposited on a titanium cylinder electrode and rinsed thoroughly with deionized water. A three-electrode gas-tight rotation cell setup was used in all electrocatalytic measurements with the cylinder as the working electrode, a 5.8 cm^2 platinum foil (Pt, 0.1 mm thick, 99.99% metal basis, Alfa Aesar) as the counter electrode, a Ag/AgCl/1 M electrode (CH Instruments, Inc.) as the reference electrode, and a solution of 0.1 M potassium carbonate at a pH of 11.68-11.72 (K_2CO_3, Sigma Aldrich, 99.995% trace metals basis) as the electrolyte. After assembling the cell, the circulating bath was used to control and equilibrate the electrolyte temperature inside the working electrode compartment. Before electrochemical measurements, high purity argon gas (Ar, Airgas 99.999%) as the inert gas or methane

gas (CH_4, Airgas 99.999%) as the reactant was flowed at a rate of 20 sccm for 30 Minutes in both the working and counter electrode compartments to prepare the gas saturated environments for electrochemical testing. These gas flow rates were maintained throughout the entirety of the electrochemical measurements. In control experiments used to understand the role of carbonate ions, instead of a 0.1 M potassium carbonate solution, a 0.1 M $KClO_4$ (≥99.99% trace metal basis, Sigma-Aldrich) electrolyte adjusted to a pH of 11.8 was used.

In the electrochemical measurements, the uncompensated resistance was determined from the system response at the high frequency (f > 100 kHz) during electrochemical impedance spectroscopy (EIS) measurements. The potential drop across the resistance of the solution from the reference electrode to the cylinder electrode was accordingly corrected. The electrochemical response of the various catalysts was determined by cyclic voltammetry at the scan rate of 10 mV s^{-1}. The long-term electrochemical oxidation of methane was conducted in the RCE cell using chronoamperometry. The overall duration of chronoamperometry was 120 minutes for the electrochemical partial oxidation of methane and multiple gas and liquid samples were taken to quantify products. The specific time of sampling is discussed and shown in the following results and discussion section. Some of the most relevant electrochemical experiments and control experiments were run by duplicate or triplicate to generate statistically significant results. Experiments that were carried only once are shown without standard deviation bars in this manuscript.

Physical characterization. Morphology and microstructure analysis of the catalyst on the cylinder electrode was carried out using scanning electron microscopy (SEM, JEOL JSM 6700 F). X-ray photoelectron spectroscopy (XPS) measurements were obtained using a Kratos Axis Ultra DLD spectrometer with a monochromatic Al Kα X-ray source (λ = 1486.6 eV) to determine element composition of the different electrodeposited catalysts as well as their oxidation state before and after testing.

Product detection and quantification. A gas chromatograph (GC) (8610C, SRI Instruments) was used for the detection and quantification of gas products. In methane partial oxidation experiments, the gas environment in the headspace of the cell was allowed to equilibrate and the first injection to the GC was made 20 minutes after the beginning of chronoamperometry measurements. Following injections were made at a 20-minute interval. Each GC run consisted of 14 minutes of running time and 6 minutes of cool-down between samples. Therefore, the gas product was sampled after 20, 40, 60, 80, 100, and 120 minutes after the beginning of the electrolysis, and each injection was used to calculate the Faradaic efficiency towards oxygen and CO and CO_2 products when generated. The detection limit for the detection of oxygen, CO and CO_2 gases is 250, 1 and 2 μA cm^{-2}, respectively.

Nuclear magnetic resonance spectroscopy (1D ^{1}H NMR 500 MHz with cryoprobe, Bruker) was used for the detection and quantification of liquid products. During the methane partial oxidation experiments, liquid aliquots were also collected at 20 minutes intervals (at 0, 20, 40, 60, 80, 100, and 120 minutes of electrolysis). Phenol (≥99.5%, Sigma-Aldrich) and dimethyl sulfoxide (DMSO, ≥99.9%, Sigma-Aldrich) were used as the internal standard for the quantification of liquid products. The internal standard was prepared by making a 52.5 mM of phenol and 2.1 mM of DMSO solution in deuterium oxide (D2O, 99.9%, EMD Millipore). Calibration of the NMR signals was done by calculating the ratio of the integration value of the signals for the different protons and the external standards for standard solutions containing known concentrations of each product. To quantify methanol partial oxidation products, all samples were prepared by pipetting 35 μL of the internal standard and 700 μL of the liquid aliquot into a new NMR tube. From the resulting 1D ^{1}H NMR spectra, the signal areas were normalized by that of DMSO, and the normalized signal areas were compared to the standard curve to calculate concentrations of liquid products during the partial methane oxidation reaction. The calibration curve for methanol is shown in Figure S2 as an example of the calibration curves obtained. Similar calibration curves were obtained for acetate and other potential products including formate, ethanol and propanol. The limit of quantification for methanol is 2.5 μM and is defined as the concentration at which the signal to noise (S/N) ratio is 10 while the limit of detection is 0.83 μM defined as the concentration at which the S/N ratio is 3.3. 128 scans were used for the acquisition of each NMR spectra.

THEORETICAL SECTION

The Vienna ab initio simulation package (VASP), version 5.4.4,[36-39] with the PBE GGA functional, [40] was used to implement periodic density functional theory (DFT) for all calculations. The projector augmented plane-wave (PAW) method was used to describe the electron-nuclei interaction. Oxide catalyst surface were modelled with periodic slabs, with supercell vectors of size 5.75 Å and a 4x4x1 Monkhorst-Pack grid was used for the k-point sampling of the first Brillouin zone. The cut-off energy for the plane wave was set at 600 eV, and the energy convergence threshold for the self-consistent-field (SCF) cycles was set at 10^{-6} eV per cell. Dispersion interactions were included according to the dDsC correction.[41-43]

Since β-CoOOH (*R3m* space group) was found to be the cobalt oxide phase that was most active under alkaline pH and oxidative circumstances, preliminary bulk full relaxation was conducted on this compound.[42, 44, 45] According to Bajdich *et al*.,[42] the reference surface slab was taken as a 2x2 supercell of the primitive surface cell cut from bulk β - CoOOH in the most active (10-14) direction. Surface defects on CoOOH could potentially play a role in catalytic activity, however, we did not consider them in our study as, in the absence of experimental information, this would require a comprehensive and involved systematic investigation, and our focus is on the dominant active site for methane transformation which is the 10-14 surface of CoOOH. Convergence in the adsorption energies and recovery of the bulk magnetic ordering of the center layers was obtained with a minimum thickness of four Co oxide layers and 30 Å of vacuum. To complete their octahedral coordination shell, each surface Co atom was liganded with one hydroxyl group, which would be expected in electrochemical conditions under liquid water.[42, 45-47] All model slabs

show two identical surface and present an inversion symmetry to cancel any dipole moment in the perpendicular direction. Only the outer atoms were allowed to relax during the surface geometry relaxations; the inside atoms (in a 2 Å large intermediate layer) and cell parameters remained fixed at the values established for the bulk β-CoOOH. These relaxations were continued until the residual forces were less than 0.02 eV $Å^{-1}$. A Fermi smearing of 0.026 eV, or 298 K in temperature, was used to calculate the electronic occupancies. To better describe the electronic structure of this high electronic correlation material, a model Hubbard Hamiltonian (designated + U) was included in the calculations. On the basis of previous works, the formalism proposed by Dudarev *et al.*[48] was used, along with the *U–J* value of 3.52 eV for the cobalt 3d electrons.[41-43]

Accounting for solvation effects was achieved by exploiting an implicit solvation model as implemented by Hennig and co-workers under the name VASPsol.[49-51] The influence of the electrochemical potential was included using the surface-charging method, with an implicit modelling of the electrolyte based on the linearized Poisson-Boltzmann (PB) equation.[50, 51] In contrast to the initial surface charging approach, which relies on a homogeneous background charge,[52] this electrolyte distribution balances the surface charge without the need for any correction terms. Hajar *et al*. have provided a more thorough explanation of the compared methods.[53]

Because we are dealing with a grand canonical description of the electrons from the surface charging methods, the energies reported in this work are free energies. The influence of the change in zero-point energy (ZPE) was found to be small in other works.[43, 45] Therefore, considering the number of intermediates, the influence of ZPE was not computed here.

RESULTS

The results section of this manuscript is organized in the chronological order in which we approached the research of methane oxidation catalysts. First, we determine the maximum methane oxidation rates achievable in our RCE cell based on the well-defined transport properties of our system. We also establish what are the maximum partial current densities for methanol and accordingly, the quantification limit of the analytical tools needed to measure methanol production in our cell. Second, we describe the deposition and physical characterization of the thin-film transition metal (oxy)hydroxides. Third, we describe the catalytic activity of transition metal (oxy)hydroxides for the partial electrochemical oxidation of methane and the results obtained during the systematic interrogation of these materials to separate the transport, electrochemical and thermochemical contributions to the experimental performance. Finally, we present our DFT study of the reaction mechanism and potential dependence, and show that there is an optimal window of potential for selective methanol oxidation.

Determination of maximum methanol production rates. In our RCE cell, the film transfer coefficient for any molecule or ion can be calculated from the Sherwood number Sh_{RCE} which is given by the relation in Equation 1[27, 35]

where Re and Sc are the Reynolds and Schmidt numbers, respectively. The average deviation from the experimentally measured Sh number with the general correlation in Equation (1) is ±7.7% for Re>500. At lower Re numbers for the RCE system, the background convection by the bubbling of the gas dominates mass transport to the surface of the electrode.[35]

$$Sh_{RCE} = \frac{k_m}{D/d_{cyl}} = 0.204 {Re_{RCE}}^{0.59} Sc^{0.33} \quad (1)$$

At a temperature of 17 °C utilized in most of the experiments in this work, the concentration of methane in solution at an overhead pressure of 1 atm of CH_4 is 1.6 mM. When the cylinder electrode is rotated between 100 and 800 rpm (corresponding to Sh_{RCE} numbers for methane of 87 and 295), the mass transport limited flowrates of methane to the surface of the electrode $J_{CH4,\,max}$ are between 1.9 and 6.3 x 10^{-9} mol cm^{-2} s^{-1} (Figure 3, top panel). At these methane transport rates, the maximum partial current densities for the partial oxidation of methane to methanol $j_{CH3OH,\,max}$, assuming a two electron oxidation process, ranges between 0.36 and 1.22 mA cm^{-2} (Figure 3, middle panel). The low partial current densities are to be expected as mass transport to the electrode is limited by external mass transport of methane from the bulk of the electrolyte, and because methane is one of the less soluble gases in water.

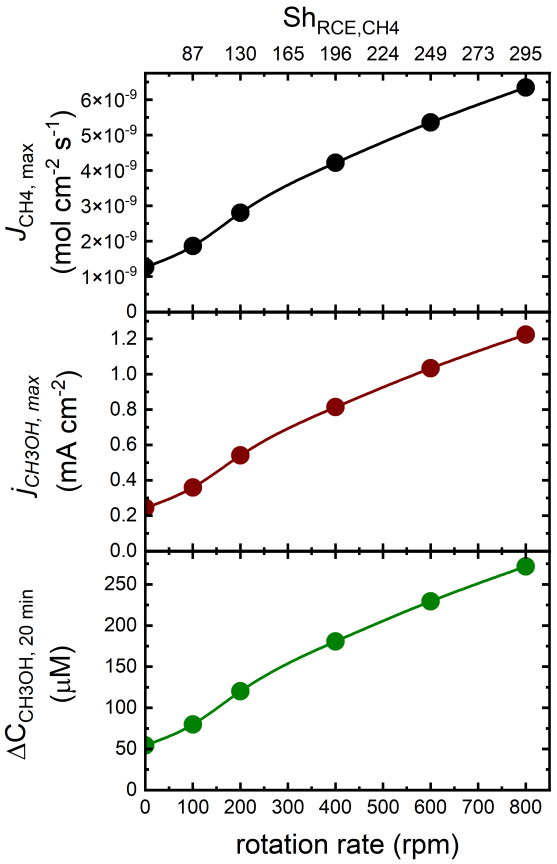

Figure 3. Mass transport limited methane partial oxidation $J_{CH4,\,max}$ with the corresponding maximum partial current densities for methanol $j_{CH3OH,\,max}$ and the maximum methanol concentration change in the electrolyte between liquid samples collected every 20 minutes $\Delta C_{CH3OH,\,20\,min}$.

In the RCE cell, a compromise is made between obtaining high partial current densities for methane to methanol oxidation and decoupling transport effects from intrinsic kinetics. Because the cylinder electrode active area is 3 cm^2 and the volume of electrolyte in the cathode compartment is 84 mL, the maximum change in concentration of methanol that can be measured over a liquid sampling interval of 20 minutes $\Delta C_{CH3OH,\,20\,min}$ is between 54 and 270 μM (Figure 3, bottom panel) for electrodes rotated at speeds between 0 and 800 rpm, respectively. This would imply that all methane reaching the electrode is transformed selectively to methanol, which is not typically observed. The 500 MHz NMR utilized for methanol quantification has a limit of detection of 0.8 μM and thus is sensitive enough to quantify methanol products in our experimental setup. Other techniques such as HPLC, have quantification limits in the order of 1 mM[31] and cannot be used to detect methanol in our system. The use of HPLC for methanol quantification in our system would require an order of magnitude larger electrode area to electrolyte volume ratio.

Electrodeposited transition metal (oxy)hydroxides. Unary transition metal (oxy)hydroxides of CoO_x, CuO_x, NiO_x, FeO_x, and MnO_x were prepared by electrodeposition as described in the experimental section.[34] Scanning electron microscopy (SEM) was used to characterize the morphology and microstructure of different transition metal (oxy)hydroxides on the surface of the titanium substrate (Figure S3) before and after electrochemical oxidation of methane for 2 hours. The titanium substrate showed a relatively flat surface after mechanical polishing and immersion in the HCl solution to remove the surface oxide. Electrodeposited cobalt (oxy)hydroxide shows the typical dense film morphology observed for electrodeposited cobalt oxides.[54] Cracking of the films is observed upon drying and the pulling of vacuum for electron microscopy. After electrochemical testing over 2 hours, some of the cobalt oxide film was lost (Figure S3b). The electrodeposited copper oxide (Figure S3c) showed angular particles before oxidation with edges and corners closely packed on the surface of the titanium substrate. The copper oxide film after 2 hours of testing appeared less densely packed while the particle edges were still well defined. Nickel (oxy)hydroxide (Figure S3d) exhibited a porous film morphology formed by small nanoplates. This nanoplate morphology was maintained after methane partial oxidation and is similar to those obtained during electrodeposition of other nickel (oxy)hydroxides.[34] Manganese (oxy)hydroxide (Figure S3e) showed larger nanoplates compared to the nickel oxide catalyst. The MnO_x film also showed cracks upon drying but maintains the nanoplate morphology. Iron (oxy)hydroxide (Figure S3f) showed a porous structure in a dense film similar to NiO_x before oxidation, while its porous microstructure could not be entirely resolved after oxidation. In general, the oxidatively electrodeposited transition metal (oxy)hydroxide films can be characterized as porous thin films while CuO_x is dense and nonporous. The slight changes in morphology between before and after testing are in line with changes observed for thin film transition metal oxides used for electrochemical water oxidation, where some of the catalyst film is lost via dissolution under the local acidic environments.[34, 54] The thickness of the catalyst films varies between a few nanometers for the films deposited with only 5 LSVs to a few hundred nanometers for the films deposited with 100 LSVs. The maximum catalyst loading achieved by oxidative electrodeposition is of less than 100 μg per cm^2 as determined by electrochemical quartz crystal microbalance measurements.[34]

The chemical compositions of the titanium substrate and the different transition metal oxides (CoO_x, CuO_x, NiO_x, MnO_x, and FeO_x) were determined using *ex situ* XPS (Figure S4). The titanium substrate signal is non-existent or very small compared to the XPS signal from the various metal (oxy)hydroxides indicating the conformal deposition of the catalysts over the cylinder geometry in the form of unary metal (oxy)hydroxides. The XPS signal from all the catalyst deposited via oxidative electrodeposition remain unchanged after testing indicating that the electrodeposited form of the (oxy)hydroxides is identical to that active for water and methane oxidation (Figure S5). Only CuO_x changes before and after testing as this catalyst is deposited via reductive electrodeposition. The titanium substrate showed signals of both metallic titanium and TiO_2. The Co 2p signal from the as-deposited and after testing CoO_x catalyst corresponds to that of cobalt in CoOOH. The acetate to cobalt ratio before and after testing does not change significantly and is in a ratio of 1 to 0.6-0.7 (Figure S5). The Ni $2p_{3/2}$ signal from the as-deposited and after testing NiO_x electrocatalyst has a Binding energy of 856 eV corresponding to high oxidations states of +3. The presence of oxide and hydroxide signals in the O 1s region indicate that the NiO_x is better described as a NiOOH. The layered nickel (oxy)hydroxide accumulates acetate in the interlayer spacing and the Ni to acetate ratio is of 1 to 0.6 in the as-prepared material and decreases to 1 to 0.3 after prolonged testing for methane partial oxidation. The high binding energy of the Mn 2p signal (642.5 eV) in the MnO_x catalyst indicates the high valence oxidation state of the Mn atom and remains similar before and after testing. The acetate content in the MnO_x catalyst is lower than in the other electrodeposited oxides and has a ratio of Mn to acetate of 1 to 0.3 before testing and decreases to 1 to 0.15 after prolonged methane electrochemical oxidation. After testing, K 2p signals are evident for the MnO_x and CuO_x samples despite washing of the electrode with abundant deionized water. The FeO_x catalyst is deposited in the form of FeOOH with an Fe to acetate ratio of 1 to 0.2. This ratio remains constant even after testing for methane oxidation. The Cu 2p signal of the as-deposited CuO_x catalyst corresponds to that of Cu_2O while that after testing corresponds to CuO. The resting oxidation states of the metal (oxy)hydroxides after testing are thus +2 for CuO_x, +2/+3 for NiO_x, +2/+3 for the CoO_x, +3 for the FeO_x, and +3 for the MnO_x. The open circuit potential for the catalyst films after methane oxidation is between 0.6 and 0.7 V vs SHE.

Electrocatalytic performances for partial methane oxidation. The electrocatalytic activities of different transition metal oxides for the electrochemical partial oxidation of methane were studied in 0.1 M K_2CO_3. Figure S6 and S7 shows the potential vs current response of the (oxy)hydroxides electrodeposited by 100 and 5 LSV cycles, respectively. Under high catalyst loading (100 LSV cycles), CoO_x

was found to be the most active among these electrocatalysts. CuO_x was the second most active electrocatalyst. Although NiO_x, MnO_x, and FeO_x are less active, their electrocatalytic performances are still higher than the titanium cylinder electrode substrate. The low activity of the MnO_x and FeO_x catalysts might be due to the high catalyst loadings and high film thickness which results in a non-conductive film.[34, 55] When lower catalyst loadings (5 LSV cycles) were used, CoO_x was still the most active catalyst (Figure S7) although the current densities are more than an order of magnitude lower compared to the film deposited using 100 LSV cycles. At lower loading FeO_x becomes the second most active electrocatalyst at high overpotentials with an activity similar to that of the NiO_x catalyst. MnO_x, on the other hand, shows a highly resistive behavior while drawing oxidative currents already at less positive potentials compared to the other transition metal (oxy)hydroxides. All the electrocatalysts show higher current densities than the titanium substrate. No efforts have been made here in normalizing activity to the electrochemical surface area (ECSA), as the ECSA cannot be determined in a reliable manner on the titanium cylinder substrate. The current-potential response of the various transition metal (oxy)hydroxide films does not change significantly under an Ar or CH_4 atmosphere although the open circuit potentials become a few millivolts less positive when the gas atmosphere is changed from Ar to CH_4. Figure S8 shows a representative current-potential response for a CoO_x film under a CH_4 and Ar atmosphere.

Product analysis of electrochemical methane oxidation reaction. Product analysis using NMR shows methanol and acetate are the major products during the electrochemical partial oxidation of methane on the various transition metal (oxy)hydroxides at a potential of 1.06 V vs SHE (Figure 4). By collecting and analyzing samples at 20-min intervals, we have observed fluctuations in the concentration of the liquid products over time. These fluctuations reveal the dynamic nature of partial oxidation studies in the RCE cell as the produced methanol accumulates in the bulk of the electrolyte and can be further oxidized over time.

Two different thickness of the various transition metals were tested. Catalysts deposited using more linear sweep cycles result in lower methanol and acetate concentrations at the same applied potential. Methanol production for films prepared by 100 LSV cycles of the different oxides are shown in Figure S9. Among all the electrocatalysts tested, CoO_x, NiO_x, MnO_x, and CuO_x are found to be active to produce methanol and acetate while FeO_x produces O_2 and the titanium substrate (TiO_x) is largely inactive. Although the FeO_x catalyst can generate reactive oxygen species and evolve oxygen, the catalyst either does not activate methane or oxidizes it completely to CO_2 which cannot be measured accurately in our system due to the dissolution of CO_2 in the alkaline carbonate electrolyte and the ubiquitous CO_2 background signal from the CO_2 and carbonate buffer equilibrium observed in the GC. Measurement of the electrolyte pH before and after testing shows a decrease in pH of between 0.08 and 0.1 pH units when methane is the reactive gas for all the transition metals including FeO_x. This pH drop is not observed when Ar is flowed through the cell in control electrolysis experiments even when the current densities are similar. The decrease in pH in the Ar control electrolysis experiments is below 0.01 pH units and within the pH meter experimental error. This suggest that methane is indeed oxidized on all the transition metal oxides under the applied potential of 1.06 V vs SHE although no significant amounts of methanol are observed for the FeO_x film. We have not made any attempts to quantify CO_2 from the decrease in pH in the electrolyte.

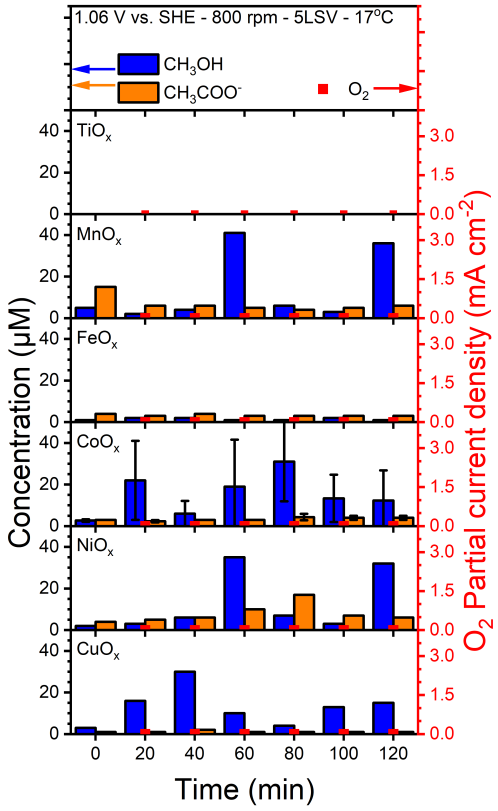

Figure 4. Production distributions of methanol and acetate on different transition metal oxides, TiO_x, MnO_x, FeO_x, CoO_x, NiO_x, and CuO_x, for electrochemical methane oxidation reaction at multiple reaction times (20 minutes intervals) within two-hours experiments using chronoamperometry performed at 1.06 V vs SHE under rotational speed: 800 rpm, catalyst loading: 5 cycles of linear sweep voltammetry, and temperature: 17°C.

Interestingly, at the beginning of the methane partial oxidation experiments (t=0 min), methanol and acetate are already detected although at low concentrations indicating that the production of methanol and acetate is thermodynamically favorable even before the application of oxidative potentials due to the likely participation of thermal reactions between the methane and the electrodeposited metal (oxy)hydroxide. Figure 5 shows the ^{1}H NMR spectra as a function of time for two experiments carried out at two different potentials for a CoO_x catalyst. Before the start of the chronoamperometry experiments, a similar amount of acetate and methanol can be observed in both experiments. These products come from the chemical reaction of methane with the electrodeposited film. At a less negative applied potential of 0.8 V vs SHE (Figure 5a), the methanol concentration remains low and fluctuates over time although the changes in concentration are not significant

while the acetate concentration increases over the first 60 minutes of the experiment and then decreases to reach again a second maximum at the end of the experiment.

At higher applied potentials of 1.06 V vs SHE (Figure 5b), the acetate concentration remained low over the duration of the experiment while the methanol concentration increased and also reached a maximum at 60 min. The methanol concentration then decreased almost to the initial values and then increased again for the last sample at 120 min. The generation of methanol and further oxidation makes the determination of faradaic efficiencies difficult as the net rates of methanol formation cannot be measured.

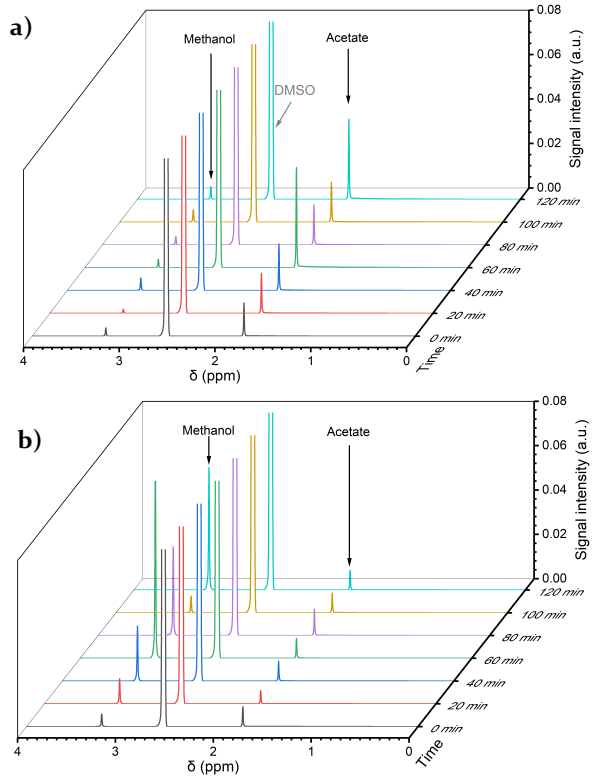

Figure 5. NMR spectra for liquid products of electrochemical partial oxidation of methane on electrodeposited CoO_x taken at 20-minute interval (a) under an applied potential: 0.8 V vs. SHE, rotational speed: 800 rpm, catalyst loading: 100 LSV, and temperature: 17°C and (b) under an applied potential: 1.06 V vs. SHE, rotational speed: 800rpm, catalyst loading: 5 LSV, and temperature: 17°C.

Control experiments to separate thermal from electrochemical contributions and potential contamination. Our first reaction after observing methanol and acetate before the application of any electrochemical bias was to check for potential sample contaminations. Seeing also methanol and acetate across most of the oxides tested prompted us to run additional control experiments. The electrodeposition bath for the oxides contained acetate so we set out to determine whether the acetate observed could come from the deposition bath and if that was the case, what concentrations could be expected. To quantify acetate carried over from the electrodeposition bath to the catalytic experiments, we dissolved three different freshly prepared cobalt oxide films (deposited using 100 LSVs) each in 2 mL of 2 M HCl and diluted the resulting solution with electrolyte until reaching the same volume as that used in the working electrode compartment of the RCE cell. We then proceeded to carry out NMR the same as any of the other samples. Figure S10a shows the result of the NMR quantification for the three dissolved CoO_x films. Indeed, concentration as high as 4 μM of acetate can be assigned to acetate trapped in the CoO_x catalyst film during electrodeposition. Importantly, no methanol was observed in the dissolved films indicating that the methanol observed before the start of the experiments comes from the reaction of methane with the catalyst film and is not due to any potential contamination arising from the liquid product quantification process. For comparison, depending on the applied potential, acetate concentrations as high as 17 μM were observed in the methane partial oxidation experiments for the CoO_x electrocatalysts deposited by 100 LSV (Figure 6a). These are concentrations almost 4 times higher than those that could be assigned to the acetate from the electrodeposition bath. NMR samples were also collected for constant potential experiments under Ar flow (Figures S10b and S10c) as a function of time. Traces of acetate were observed for the Ar control experiments in agreement with the acetate concentrations expected to come from the catalyst electrodeposition bath while methanol was not observed. Figure S10b shows a representative NMR spectra for control experiments run under an Ar atmosphere at an applied potential of 0.86 V vs SHE. The absence of the methanol signal in the NMR spectra confirms that methanol is only produced when methane is present in the system. Control experiments under Ar were run in triplicate and the average concentration of acetate as a function of time was averaged and plotted in Figure S10c. Concentrations of acetate below 5 μM at the beginning of the experiment and over the two hours of experiment under Ar flow can thus be assigned to acetate from the electrodeposition bath.

Since methanol is not generated in experiments carried out without the use of methane, we proceeded to understand the origin of the methanol observed at the start of each experiment before the application of potential. Indeed, thermal reaction of methane with surface oxides has been suggested as the rate limiting step in methane activation even for electrochemical based reactions with minimal applied potential dependence.[33] The large number of reports that imply faradaic efficiencies for methane partial oxidation above 100% also lead us to think that methane can be chemically reacting with activated oxide sites in the catalyst film. To determine whether this is unique to our oxidative electrodeposited catalysts, we ended the linear sweeps used during electrodeposition not at the most positive potential of 1.1 V vs Ag/AgCl but at the less anodic potential of 0.8 V vs Ag/AgCl where the electrodeposited films are at a less oxidized state. It is well known that the transition metal oxides of cobalt, copper, iron, manganese, nickel and titanium are electrochromic and that these electrochemically oxidized materials can store high oxidation states over long periods of time. In effect, when the electrodeposition of the film was ended at the less oxidative potential of 0.8 V vs Ag/AgCl, these films did not show significant methane oxidation products in control experiments with no applied potential (Figure S11a). Concentrations of methanol of just up to 5.6 μM were observed. In

comparison, when the electrodeposition of the film was ended at 1.1 V vs Ag/AgCl, methanol concentration of up to 22 μM where observed for experiments with no applied potential (Figure S11b). Importantly, the fluctuations in concentrations over time were also observed with methanol disappearing after 80 minutes of experiment without any applied potential. This indicates that the electrodeposited films store high oxidation states and that these states are trapped for periods of times long enough for the film to be washed with deionized water and dried after electrodeposition and left on the bench of the lab under an air environment until the start of the methane oxidation experiments in the RCE cell. Indeed, these oxidation states are long lived and active enough to drive thermochemical methane oxidation upon being put in contact with the dissolved methane. It is also likely that the only mechanism for the reduction of the high valence oxidation states in the electrodeposited films is by reacting with methane. For comparison, Figure S11c shows three similar CoO_x catalysts tested at an applied potential of 1.06 V vs SHE. Under these conditions, concentrations of up to 53 μM are observed in one of the experiments while in the other two experiments the maximum methanol concentrations were 43 and 45 μM. Therefore, up to half of the methanol produced can be assigned to the thermal oxidation of methane by high oxidation states in the as-prepared CoO_x catalyst. We hypothesize that this is not unique to our catalysts and could explain the Faradaic efficiencies of over 100% for methane electrochemical oxidation observed in other systems. Non-electrochemical transformation of methane to methanol under open circuit conditions at temperatures of 300 °C or higher have been previously reported to proceed via redox cycles on transition metal oxides where methane is oxidized by active oxygen species formed on the catalyst surface.[56] The contribution of non-electrochemical methane oxidation processes, however, is rarely considered as a possibility in ambient temperature electrochemical cells.

In order to gain a better fundamental insight of the electrochemical and thermal steps involved in the partial oxidation of methane, the effects of various factors including applied potential, operating temperature, catalyst loading, electrolyte compositions, and rotational speed on methanol selectivity were systematically studied. Since cobalt oxide (CoO_x) is a well-known catalyst with methane partial oxidation activity, well-characterized redox properties, and active oxygen species,[34, 55] we have selected it as a prototypical electrocatalyst to understand mass, charge and heat transport phenomena involved in methane partial oxidation.

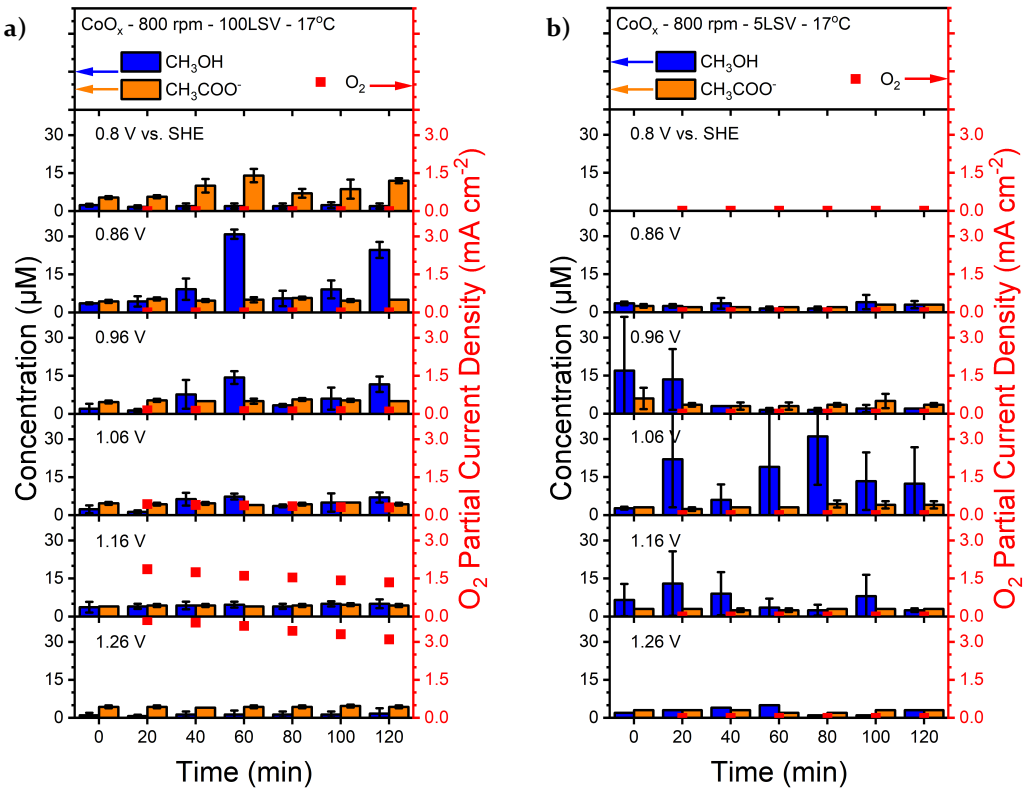

Figure 6. Production distributions of methanol and acetate on cobalt oxides, CoOx, for the electrochemical partial oxidation of methane at multiple reaction times (20 minutes intervals) within two-hours experiments using chronoamperometry performed at different applied potentials: 0.8, 0.86, 0.96, 1.06, 1.16, and 1.26 V vs SHE under rotational speed: 800rpms, temperature: 17°C with (a) catalyst loading: 5 cycles of linear sweep voltammetry and (b) catalyst loading: 100 cycles of linear sweep voltammetry.

Catalyst loading (porosity). In our setup, the amount of electrodeposited transition metal (oxy)hydroxides can be controlled by changing the number of electrodeposition cycles.[34] The loadings of the catalytic film as well as its morphology and conductivity is expected to affect the degree of electrochemical oxidation of methane and its overoxidation. Higher porosity is expected to increase the tortuosity

for the transport of methanol out of the catalyst film. Two different catalyst loadings (deposited by 5 and 100 LSVs) were used to explore the relationship between methanol selectivity and mass and charge transport phenomena within the catalyst film.

Low catalyst loadings corresponding to thinner catalyst films require applied potentials of at least 0.96 V vs SHE to activate methane and accumulate methanol in the RCE cell at concentrations of at least 10μM (Figure 6b). At less oxidative potentials (0.8~0.86 V), only trace amounts of methanol and acetate are detected. The detection of appreciable amounts of methanol only occur at potentials of 0.96 to 1.16 V vs SHE, and more positive potentials lead to the overoxidation of methanol. In comparison, the thicker catalyst film obtained through the deposition of the CoO_x film with 100 LSV required more modest potentials (0.8~0.86 V vs SHE) to activate and oxidize methane (Figure 6a). As the potential was biased to more oxidative windows, the concentration of methanol and acetate substantially decreased until methanol is only present at trace amounts. The onset for the oxygen evolution reaction also requires lower overpotentials for the thicker films in agreement with the OER literature where cobalt has been shown to be active across the bulk phase of the catalyst film.[57, 58] Therefore, thicker catalyst films or more catalyst loadings lead to both faster methane activation at low overpotentials as well as higher methanol overoxidation at high overpotentials. Higher overoxidation of methanol at potentials of 1.06 V vs SHE for the thicker film compared to the thinner film is due to the highly porous structures and thus the longer paths for methanol to exit the thicker catalyst layer. The trapping of bubbles on the catalyst films was not observed at the potentials tested. In any future application, an optimal point between applied potential and catalyst thickness must be determined for porous transition metal (oxy)hydroxides if these are to be used as catalyst for the methane to methanol transformation.

Applied potential. The driving force for the partial oxidation of methane and the overoxidation of methanol changes as the applied potential is increased. At low applied potentials of around 0.8 V vs SHE, acetate is preferentially accumulated in the electrochemical cell for the thicker CoO_x films (Figure 6a). This indicates that although the activation of methane occurs readily, the activated methane intermediate likely reacts with the carbonate or the CO_2 generated from the complete oxidation of methane to produce acetate. At potentials higher than 0.86 V vs SHE, the selectivity changes to methanol reaching a maximum accumulation of methanol at intermediate overpotentials. Higher overpotentials lead to the complete oxidation of methanol as corroborated by the decrease in the pH at the end of the experiments while the pH does not change in experiments under Ar flow. Higher applied potentials indeed modify the density of high valence oxidation states available for catalysis which are also needed to conduct charges in the porous transition metal (oxy)hydroxide films. Therefore, electrochemical partial oxidation of methane to methanol should be more favorable at relatively intermediate overpotentials where enough of the higher oxidation states of the catalysts are present on the surface of the catalyst but before the oxygen evolution reaction becomes dominant at high overpotentials.

Electrolyte composition. An emerging question is whether carbonate ions fulfill the role of mild oxidants and oxygen atom donors during the oxidation of methane. To determine if carbonate ions are indeed needed for the oxidation of methane to acetate and methanol, control experiments were carried out in a potassium perchlorate electrolyte with pH adjusted to that of the carbonate electrolytes (pH=11.8). Figure S12 shows the product distributions at two potentials for a 100 LSV CoO_x film. The production of acetate and methanol is similar as those in experiments with the carbonate electrolyte. Therefore, is safe to conclude that carbonate ions are not the predominant oxygen donor sources during methane electrochemical partial oxidation in transition metal (oxy)hydroxides and are not involved in the reaction mechanism.

Rotation speed. The RCE cell allows the study of electrocatalytic reactions under well characterized mass transport. The effect of the rotation of the electrode in the methane partial oxidation rates has also been considered here. By tuning the rotation of the electrode, mass transport can be systematically changed to modify the thickness of the boundary layer for the transfer of reactants and intermediates in and out of the electrocatalytic surface.

As shown in Figure 7a, the highest concentrations of methanol during the two-hours experiments at rotation speeds of 0, 100, 400, and 800 rpms are 33, 42, 46, and 55 μM, respectively. Lower rotation speeds or static electrodes are limited by mass transport of methane to the electrode surface which leads to the accumulation of lower concentrations of methanol in the cell. However, the concentration of the methanol accumulated in the cell remains rather constant and does not fluctuate as much as for higher rotation speeds. The electrolyte volume in the working electrode compartment is 84 mL while the electrode area is just 3 cm^2. Under low rotation speeds, the methanol accumulated is not forced to pass by the electrode surface preventing its further oxidation. On the other hand, while higher rotation speed contributes to higher methanol concentrations by ameliorating the mass transport of methane to the electrode, it also contributes to the faster further oxidation of methanol resulting in large fluctuations in the methanol concentrations observed as a function of time. The rather constant concentration of methanol observed at low rotations speeds is what would be expected in a system with two consecutive reactions where the methanol is the reaction intermediate. At some time, the rate of methanol production should match that of methanol overoxidation and reach a steady-state concentration. This makes the cyclic nature of the concentration of methanol at higher rotations speeds difficult to rationalize. An important metric can still be obtained by measuring the maximum change in methanol concentration in the 20 minutes sampling interval as the maximum mass transport limited rate of methanol production in the RCE cell under the different rotations is well characterized as shown in Figure 3. At rotations speeds of 100 rpm, equivalent to a $Sh_{RCE,CH4}$ value of 87, changes in concentration of as much as 28 μM of meth-

anol are observed in the 20-minutes interval between samples which approaches half of the maximum methanol production rate possible, indicating that close to 50% of the methane reaching the surface of the electrode is transformed effectively to methanol (Fig. 7b).

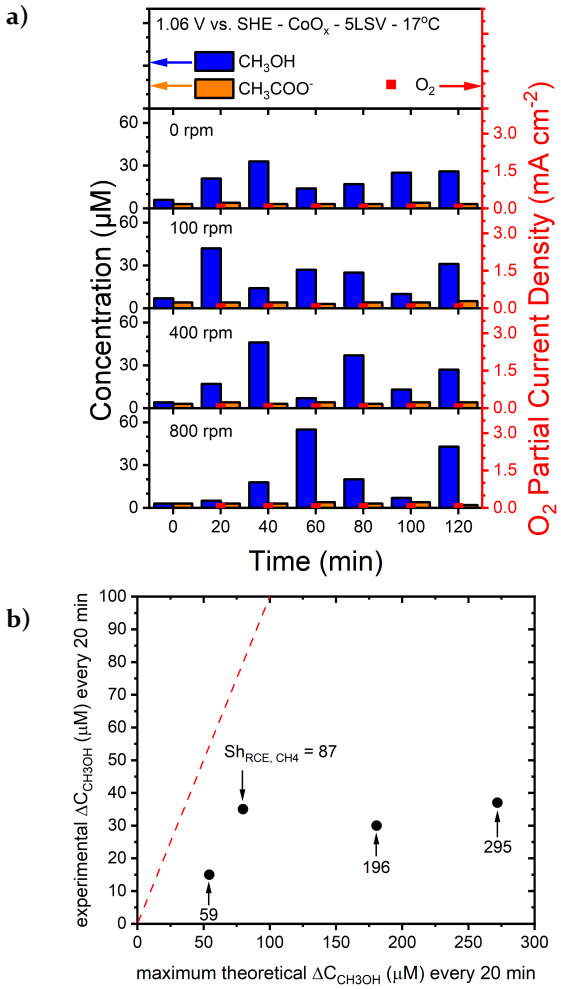

Figure 7. (a) Production distributions on cobalt oxides, CoOx, for electrochemical partial oxidation of methane at multiple reaction times (20 minutes intervals) within two-hours experiments using chronoamperometry performed at 1.06 V vs SHE under different rotational speed: 0, 100, 400, and 800rpms, catalyst loading: 5 LSV, and temperature: 17°C. Current vs potential curves are shown in Figure S14. (b) Experimental versus maximum theoretical methanol accumulation rates (red dotted line) in the RCE cell.

At this time, the reason for the fluctuation of the methanol and acetate concentrations as a function of time is not clear. Methanol is never observed in the cathode compartment so we disregard the possibility for time dependent transport or crossover of methane-derived species back and forth between the anode and the cathode compartments (Figure S13). Only trace amounts of acetate below the limit of quantification are observed in the cathode compartment as these charged species can be transported through the anion conductive membrane. Acetate, however, is the minority charge carrier in the alkaline electrolyte. Computer fluid dynamics of the electrolyte in the RCE cell indicate the formation of different convection zones in the cell.[35] As expected, the energy introduced through the rotation of the electrode is mostly dissipated within the hydrodynamic boundary layer of a few hundred micrometers around the rotating cylinder electrode. Over time, this energy is transferred to the bulk of the electrolyte increasing the convection in the cell. Convective patterns are disrupted by the bubbling of methane inside the electrolyte and by the interactions between the electrolyte and the walls of the cell. The dissipation of mechanical energy in the cell can indeed be reflected in the periodicity of the changes in the concentration of products but at this time these relations are purely speculative. Further multi-scale modeling of the reactor is expected to shine light into the relation between electrode rotation and product accumulation. We highlight that understanding of mass transport is of the outmost importance for the study of methane to methanol systems. The study of the direct oxidation of methane to methanol has been comprehensively investigated over the past decade; however, little research has taken mass transfer effects into account.

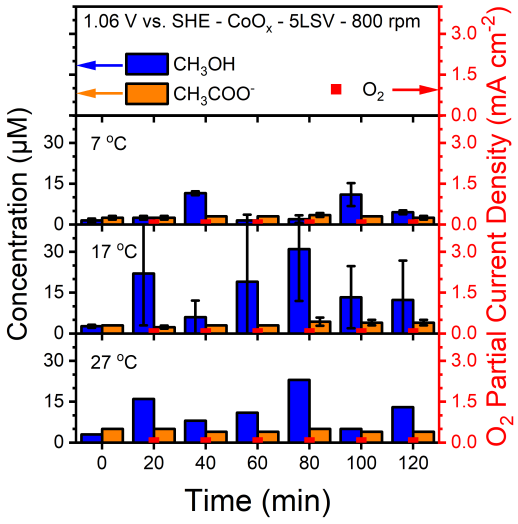

Figure 8. Temperature dependence of the production distributions of methanol and acetate on cobalt oxides, CoO_x, for electrochemical partial oxidation of methane. Samples are collected at 20 minutes intervals within a two-hours experiment. Chronoamperometry is performed at 1.06 V vs SHE under rotational speed of 800rpms, catalyst loading: 5 cycles of linear sweep voltammetry, and different temperature: 7, 17, and 27°C. Current vs potential responses at various temperatures are shown in Figure S15.

Operating temperature. The rate-limiting step in methane electrochemical oxidation can be the regeneration of the catalytic site, the transport of methane to the catalyst surface, the thermal activation of the C-H bond and its hydroxylation, or the desorption and removal of the methanol (Figure 1). Any of these processes is expected to be a function of temperature as higher temperatures can increase charge hoping in conductive oxides, the diffusion coefficient of methane in liquids, as well as increase the rates of methane activation and the endothermic desorption of methanol. Higher temperatures can also increase the rate of methanol overoxidation and thus temperature can be expected to have a complex effect on methane electrocatalysis. Figure 8 shows the dependence of the product

distribution during the methane partial oxidation as a function of temperature. Three different temperatures were studied ranging from 7 to 27°C to try and understand the role of thermal processes in the activation of methane and the overoxidation of methanol. Linear sweep voltammetry of the CoO_x catalyst at the different temperatures are shown in Figure S15. Higher temperatures correlate with higher current densities. At a lower operating temperature (7°C), the accumulation of methanol in the cell is lower potentially due to slower kinetics for methane oxidation as mass transport of methane to the surface at 800 rpm is not limiting. At lower temperature less thermal energy is available to overcome the activation barrier for C-H activation. At higher temperatures, the solubility of methane in the electrolyte decreases and could result in mass transport limitations although the diffusion coefficient for methane increases and the kinetics for both methane activation and methanol overoxidation could also increase. At temperatures of 17 and 27°C we indeed observed higher accumulation of the methanol and acetate products with higher concentrations reached at the intermediate temperature of 17°C. Moderate temperatures could be optimal for the transformation of methane to methanol to facilitate methane activation while limiting methanol overoxidation. The issue of the decrease in solubility of methane at higher temperatures can be circumvented either through the use of gas diffusion electrodes[59] or the application of higher partial pressures of methane.

Reaction mechanism via DFT calculation. To understand the mechanism during the electrocatalytic methane oxidation process, DFT simulations were performed. The reaction mechanism and thermodynamic analysis are shown in Figure 9. The focus is on the main reaction pathway for methane to methanol and CO_2, while the side reaction dealing with acetate formation was not explored as it is the major product only in a very narrow potential window for the thicker CoO_x film. Understanding the Cobalt oxide stability in reaction conditions is the first step in this process. CoOOH is the most stable phase for Cobalt oxide that is observed in the potential range of U = 0.5 to 1.5 V vs SHE at highly alkaline pH.[41, 42] Therefore, we consider that the catalyst is CoOOH as soon as the potential reaches 0.5 V vs SHE. Experimentally, the formation of CoOOH was achieved by activating the surface by performing CV measurement and reaching potentials more positive than 0.5V vs SHE. The open circuit potential for CoO_x films after deposition and electrochemical activation were indeed between 0.55 and 0.75 V vs SHE depending on the final potential applied during the activation cycle. The open circuit potentials also change upon the switch of the atmosphere from argon to methane. The activated surface then can perform partial oxidation of methane via the electrochemical reaction between methane and high oxidation states of the catalyst, even without an applied potential.

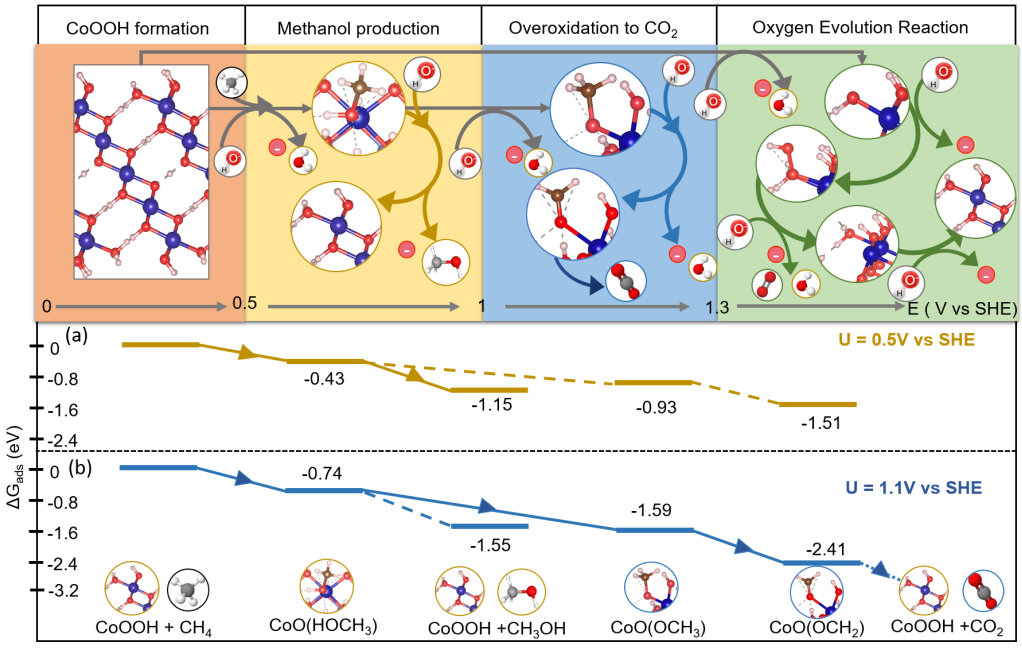

Figure 9. Reaction mechanism and reaction energy diagram at (a) U = 0.5 V vs SHE (b) U = 1.1 V vs SHE. The top panel shows the most favorable reactions at certain electrochemical potential windows. In the red box the CoOOH formation takes place starting from 0.5 V vs SHE.[42] The yellow box shows methanol production in the potential range of 0.5 – 1 V vs SHE after which the most favorable reaction would be the overoxidation of methane to CO_2 competing with the oxygen evolution reaction starting from U = 1.3 V vs SHE. The reaction diagrams are evaluated at pH = 12.

Understanding the thermodynamic branching between various reaction mechanisms when the electrochemical potential is modified then becomes the primary objective of this section of the work. As CoOOH is only stable in the potential range of 0.5 – 1.5 V vs SHE at alkaline pH we have studied the various reactions in the same potential range. From our calculations, three main reaction mechanism are at play, the predominant one depending on the potential, as shown in Figure 9:

(a) Selective methane oxidation to methanol.

$$^{*}OH + CH_4 + OH^- \rightarrow CH_3OH + H_2O + e^- \quad (2)$$

$$^{*}CH_3OH + OH^- \rightarrow CH_3OH + {}^{*}OH + e^- \quad (3)$$

$$^{*}CH_3OH + OH^- \rightarrow {}^{*}OCH_3 + H_2O + e^- \quad (4)$$

In the initial potential window of 0.5 – 1 V vs SHE, where methanol formation is favored, the first reaction step is to activate the C—H bond of methane, and this happens electrochemically on the hydroxyl group of the CoOOH surface (Equation 2). Here, surface adsorbed species are labeled with an asterisk (∗). Figure 9 (yellow zone) shows the reaction diagram of methane oxidation to methanol. At 0.5 V vs SHE (Figure 9a), we observe the electrochemical methane activation to be thermodynamically favorable (-0.43 eV). This step (Equation 2) combines electrochemical activation of the C-H bond of methane with OH^- and concerted rebinding of the CH_3 fragment with a surface adsorbed OH (*OH). The formed adsorbed $^{*}CH_3OH$ on the surface has two options (1) the CH_3OH group on the surface can desorb and the hydroxyl group on the surface can be replenished electrochemically by hydroxyl ion to give back the initial catalyst (CoOOH), represented in Equation 3. (2) the $^{*}CH_3OH$ can further oxidize to $^{*}OCH_3$ (Equation 4). We have studied both possibilities and observe that the selectivity between the two reaction is potential dependent. At lower overpotential (< 1V vs SHE), electrochemical desorption of methanol is thermodynamically favorable (Figure 9a). As we move toward more positive potential (> 1 V vs SHE), the methanol oxidation to $^{*}OCH_3$ becomes more favorable. This can be seen on Figure 9b, where the potential (1.1 V) is just above 1 V, and the $^{*}OCH_3$ species (ΔG_{ads}= -1.59 eV) is becoming more stable than desorbed methanol and hydroxylated CoOOH surface site (-1.55 eV). Increase in potential causes the H on the methanol attached to the surface to become more acidic, which then reacts with a OH^- in the solution to produce $^{*}OCH_3$ and water, which actively encourages the oxidation of $^{*}CH_3OH$. At 1 V vs. SHE, the thermodynamic favorability of the two reactions switches. Thus, thermodynamics informs us that CoOOH behaves as an excellent catalyst for the selective oxidation of methane into methanol at an intermediate window of potential (0.5 – 1 V versus SHE), which is in good agreement with our experimental observations.

(b) Methane overoxidation to CO_2.

$$^{*}OCH_3 + OH^- \rightarrow {}^{*}OCH_2 + H_2O + e^- \quad (5)$$

$$^{*}OCH_2 \rightarrow \cdots \rightarrow CO_2\ evolution$$

As already mentioned above, if we go towards a sufficiently large overpotential, the surface methanol is overoxidized to $^{*}OCH_3$ (above 1 V vs SHE, Figure 9 blue zone), $^{*}OCH_3$ then oxidizes to $^{*}OCH_2$, a step again thermodynamically favorable (Equation 5). These are the first steps toward the overoxidation of methane to CO_2 which is captured as carbonate in the alkaline electrolyte. The other favorable oxidation steps after $^{*}OCH_2$ were not explicitly calculated here.

(c) Oxygen evolution reaction

$$^{*}OH + OH^- \rightarrow {}^{*}O + H_2O + e^- \quad (6)$$

$$^{*}O + OH^- \rightarrow {}^{*}OOH + e^- \quad (7)$$

$$^{*}OOH + OH^- \rightarrow {}^{*} + O_2 + H_2O + e^- \quad (8)$$

$$OH^- + {}^{*} \rightarrow {}^{*}OH + e^- \quad (9)$$

Finally, at sufficiently large overpotentials, we will observe the oxygen revolution reaction which would be directly competing with methane overoxidation to CO_2. The reaction mechanism for OER in alkaline conditions is given in the Equations 6-9. OER reaction on CoOOH has been extensively studied in the literature.[41-43] We find that the OER occurs at a potential on 1.28 V vs SHE in pH = 12 with the rate determining step (RDS) as the desorption of O_2 (Equation 8). This matches very well with what has already been reported by Curutchet *et al*.[45]

The competition between the OER process and the methane oxidation reaction for the active site is an essential element to consider in the reaction condition. Methane activation can interfere with OER intermediates at two different reaction stages. First, as seen above, surface *OH can be used to form $^{*}OHCH_3$ (Equation 2), preventing their conversion into *O (Equation 6). Second, *O intermediates might interact with methane and OH^- to form $^{*}OCH_3$ (Equation 10), preventing the formation of *OOH (through Equation 7).

$$^{*}O + CH_4 + OH^- \rightarrow {}^{*}OCH_3 + H_2O + e^- \quad (10)$$

Both reactions occur at high overpotentials and are thermodynamically favorable. For example, Equation 2 will have a ΔG of -0.8 eV at a potential of 1.3 V vs SHE, but Equation 6 will have a ΔG of -0.15 eV. Similarly, equation 10 will have a ΔG of -1.4eV at the same potential but equation 7 will only have a ΔG of -0.1 eV. In any scenario, the two competing reactions mentioned above will have a significant impact on OER but have no impact on the formation of methanol at moderate overpotentials.

RESULTS AND DISCUSSION

From a thermodynamic perspective, the electrochemical partial oxidation of methane to methanol in alkaline electrolytes (Equation 11) requires a relatively low oxidative potential of only 0.18 V vs SHE at pH 14 compared to the oxygen evolution reaction (OER, Equation 12) which requires an additional 0.22V. Despite methane partial oxidation to methanol being thermodynamically accessible in an electrochemical cell, this reaction is kinetically difficult and requires an adequate catalyst to reduce activation energy and a large overpotential to drive measurable partial current

densities. Driving large enough currents often requires biasing the electrode to oxidative potentials at which oxygen evolution also takes place despite this reaction also being kinetically slow.

$$CH_4 + 2OH^- \rightleftharpoons CH_3OH + H_2O + 2e^- \; E^0 = 0.18V \qquad (11)$$

$$2OH^- \rightleftharpoons 0.5O_2 + H_2O + 2e^- \qquad E^0 = 0.40V \qquad (12)$$

At very high oxidative potentials, the oxygen evolution reaction outcompetes the methane oxidation reaction and oxygen or CO_2 are predominantly formed.[31] An often ignored fact is that high overpotentials are also needed to transport charges on porous oxide electrodes as these materials are electrically insulating and become conductive only when the population of high oxidation states in the catalyst film is high.[34, 60] This means that we cannot expect to see methane activation until transition metal (oxy)hydroxides become oxidized and conductive.

The first point is to form on the catalyst surface the right oxidation number at the considered transition metal for electronic conductivity and methane oxidation. Figure 10 shows the ranges of applied potentials vs SHE at which electrodeposited transition metal (oxy)hydroxides[34, 61] become conductive by changing the valence state from +2 to +3 for the Co, Ni, Fe, and Mn (oxy)hydroxides in 1 M KOH. At potentials positive of the water oxidation potential (0.4 V vs SHE in pH 14), many of these metal (oxy)hydroxides enter higher oxidation states and become active for both the methane partial oxidation reaction and the oxygen evolution reaction requiring somewhere between 250 and 500 mV overpotential to sustain meaningful oxidative currents.[34]

From a purely experimental perspective, the potential window between 0.5 and 1.0 V vs SHE is thus optimal to enable any of the transition metal (oxy)hydroxides to be conductive while accessing a large population of metal-oxo sites on the surface of the catalysts to activate and oxidize methane. It must be noted, however, that the redox potentials in Figure 10 and the rates of water oxidation are a function of pH and will change in a different manner for each metal (oxy)hydroxide relative to the 0 V vs SHE.[62] That is, the onset of conductivity and the population of high oxidation states on the surface of the catalyst during operation is a complex function of the potential and the local pH. Based on previous theoretical works for the activation of methane,[63, 64] and on the DFT results on CoOOH presented here, we hypothesize that indeed various transition metal oxides are active for the transformation of methane to methanol at ambient and moderate temperatures provided four conditions are met: 1) enough methane is supplied to the catalyst surface, 2) the transition metal oxide is conductive without the need of large overpotentials where OER could become dominant, 3) the potential is low enough so that methanol can be preferentially desorbed versus the formation of methoxy and further oxidation, and 4) the catalyst architecture and the transport properties of the cell allow methanol to be transported away from the electrode before it can be further oxidized. Indeed, our DFT calculations on CoOOH show for a potential below ~1 V, desorption of methanol coupled with adsorption of OH^- on the Co site is thermodynamically favored versus further oxidation to methoxy, so that electrocatalytic oxidation with the control of the potential could open a possibility of selective formation of methanol. Moving to gas phase humidified membrane electrode assemblies could be a viable approach to electrochemical methane-to-methanol transformation systems provided the four conditions above of high methane transport, high metal oxide catalyst conductivity, fast methanol desorption relative to overoxidation, and fast methanol product collection are met.[65-67]

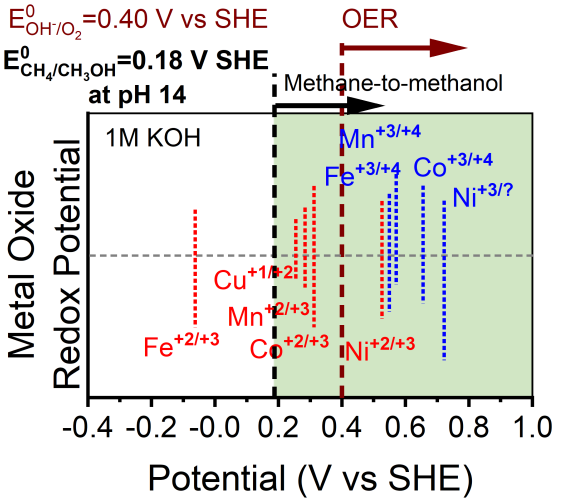

Figure 10. Redox potentials experimentally measured for oxidatively electrodeposited transition metal (oxy)hydroxide in 1 M KOH.

We have shown here that partial oxidation of methane proceeds via the chemical reaction between methane and high oxidation states of the catalyst, even without an applied potential beyond the one needed to maintain the oxidation state of the catalytic site. Faradaic efficiency may then no longer be a good descriptor for selectivity in the partial oxidation of methane to methanol. We consider the following steps for the partial oxidation of methane on metal-oxo sites. At intermediate overpotentials (0.5 - 1 V vs SHE), the methane is activated electrochemically by dissociation of a C-H bond via reaction with a hydroxyl anion and concerted rebinding with a hydroxyl located on the surface of the electrode to form adsorbed methanol (Equation 2). Methanol can desorb from the site, and this reaction is made exothermic by a concerted electrochemical adsorption of OH^-. At larger overpotentials (1 - 1.3 V), the hydroxyl group attached to the methanol on the surface becomes acidic leading to the formation of methoxy which subsequently overoxidizes to CO_2 which is captured as carbonate in the alkaline electrolyte. At even higher overpotentials (>1.3 V), the oxygen evolution process becomes a competitive reaction as well.

According to thermodynamics of the reactions, methane overoxidation to CO_2 by methoxy formation would be preferable over OER. A significantly greater methane concentration might result in a drop in OER and an increase in overoxidation since both processes utilize the same active site. However, at moderate methane concentration not all active sites would be occupied/deactivated by methoxy, hence we would observe significant OER on the CoOOH surface at large overpotentials.

CONCLUSIONS

In summary, we have demonstrated the use of electrochemical methods for the deposition of a family of thin-film transition metal (oxy)hydroxides, which is a simple, clean, and efficient strategy for the fabrication of electrodes for the partial oxidation of methane to methanol in a carbonate electrolyte. CoO_x, NiO_x, MnO_x and CuO_x are active for the partial oxidation of methane to methanol while FeO_x oxidized methane entirely to CO_2 in the potentials tested. Taking CoO_x as a prototypical methane partial oxidation electrocatalyst, the dependence of activity and methanol selectivity on catalyst loading (porosity), applied potential, temperature, and cell hydrodynamics were systematically investigated. Higher catalyst loading with thicker films lead to more significant overoxidation of methanol due to the highly porous structures and thus the longer paths for methanol to exit the catalyst layer. Acetate is a side-product at low overpotentials (0.8 V vs SHE) while methanol is the favored product at medium overpotentials (0.86~1.06 V vs SHE). This very interesting potential regime where selective oxidation of methane to methanol is seen is confirmed and explained by our DFT simulations. We find an optimum potential window in which methane activation forming methanol and methanol desorption are both thermodynamically favorable on fully hydroxylated CoOOH. Methanol desorption from the site is favored due to the stabilizing concerted electrochemical adsorption of a OH^- from the solution. The selectivity is hence explained by competitive adsorption with hydroxide anion, which expels the methanol from the site, and by the transport of methanol away from the electrode. High overpotentials (above 1.16 V vs SHE) result in the overoxidation of the produced methanol to CO_2, since electrooxidation of methanol to methoxy becomes more favorable than its desorption, and the production of oxygen through OER. Similar mechanisms for the production of methanol could be at play on other unary transition metal (oxy)hydroxides and need to be systematically studied through a combination of experiments under well-defined transport conditions and DFT simulations.

The temperature also plays an essential role in both methane activation and overoxidation of the produced methanol. High temperatures result in lower selectivity for methanol likely to the increase in the rates of thermal steps for both methane activation and methanol overoxidation, as well as the increase in the OER activity and the decrease in solubility of methane in the electrolyte. Higher rotation speeds of the cylinder electrode increase turbulence in the cell and decrease the cycling time of the accumulation and overoxidation of methanol in the electrochemical cell. More importantly, catalyst loading (porosity) and electrolyte convection are both correlated with the effect of mass transfer, implying the importance of understanding mass transport of the relevant species in partial oxidation studies of methane.

Through the use of the gas-tight rotating cylinder electrode cell, unique conditions of hydrodynamics for the partial oxidation of methane show the importance of the control on both kinetics and mass transfer of each step during the reaction. Consequently, this work demonstrates electrodeposition as a viable strategy for catalyst fabrication and may pave the way for efficient strategies of catalyst preparation for further studies of the electrochemical partial oxidation of methane under ambient conditions as well as well-defined conditions of mass, heat, and charge transport.

The transition metal (oxy)hydroxide catalysts reported here should enable the decentralized production of methane to methanol utilizing electrochemical units engineered for optimal methane delivery to the electrode surface as well as rapid methanol product removal and collection. Modular electrochemical devices with advanced electrode architectures for methane and methanol transport can one day enable the efficient and decentralized partial oxidation of methane to methanol at ambient temperatures. In this work we have provided a first understanding of how to tackle the design of these devices.

ASSOCIATED CONTENT

Supporting Information. Additional data for control experiments and characterization of materials is presented in the supporting information. This material is available free of charge via the Internet at http://pubs.acs.org.

AUTHOR INFORMATION

Corresponding Author

* Carlos G. Morales-Guio. Department of Chemical and Biomolecular Engineering, University of California, Los Angeles, CA 90095, United States. Email: moralesguio@ucla.edu

Author Contributions

[†]K.S. and S.K. contributed equally to this work.
The manuscript was written through contributions of all authors. All authors have given approval to the final version of the manuscript.

Notes

A provisional patent has been filled related to this work.

ACKNOWLEDGMENT

C.G. M.-G. acknowledges financial support from a Scialog program sponsored jointly by Research Corporation for Science Advances and the Alfred P. Sloan Foundation and includes a grant No. G-2021-14160 by the Alfred P. Sloan Foundation. S.K. and P.S. acknowledge financial support from the National Science Foundation grant 2140374. This work also used computational and storage services associated with the Hoffman2 Shared Cluster provided by the

UCLA Institute for Digital Research and Education Research Technology Group. This research used the resources of the National Energy Research Scientific Computing Center (NERSC), a U.S. Department of Energy Office of Science User Facility operated under Contract No. DE-AC02-05CH11231. The authors want to thank XSEDE SDSC s Comet, Expanse Supercomputer, and Bridges PSC for the computation time.

REFERENCES

1. Jang, J.; Shen, K.; Morales-Guio, C. G., Electrochemical direct partial oxidation of methane to methanol. *Joule* **2019,** *3* (11), 2589-2593.
2. Global Gas Flaring Reduction Partnership (GGFR). http://www.worldbank.org/en/programs/gasflaringreduction (accessed 2023-02-14).
3. IEA. Industry 2022. https://www.iea.org/reports/industry (accessed 2023-02-14).
4. Energy Transitions Commission. Mission Possible: Reaching net-zero carbon emissions from harder-to-abate sectors by mid-century. 2018. http://www.energy-transitions.org/mission-possible (accessed 2023-02-14).
5. IRENA and Methanol Institute. Innovation Outlook: Renewable Methanol, International Renewable Energy Agency, Abu Dhabi. 2021. https://www.irena.org/publications/2021/Jan/Innovation-Outlook-Renewable-Methanol (accessed 2023-02-14).
6. Soucie, H.; Elam, M.; Mustain, W. E., Practical Assessment for At-Scale Electrochemical Conversion of Methane to Methanol. *ACS Energy Lett.* **2023,** *8* (2), 1218-1229.
7. Yuan, S.; Li, Y. D.; Peng, J. Y.; Questell-Santiago, Y. M.; Akkiraju, K.; Giordano, L.; Zheng, D. J.; Bagi, S.; Roman-Leshkov, Y.; Shao-Horn, Y., Conversion of Methane into Liquid Fuels-Bridging Thermal Catalysis with Electrocatalysis. *Advanced Energy Materials* **2020,** *10* (40), 2002154.
8. Mostaghimi, A.; Al-Attas, T.; Kibria, M.; Siahrostami, S., A review on electrocatalytic oxidation of methane to oxygenates. *Journal of Materials Chemistry a* **2020,** *8* (31), 15575-15590.
9. Shah, M.; Oh, C.; Park, H.; Hwang, Y.; Ma, M.; Park, J., Catalytic Oxidation of Methane to Oxygenated Products: Recent Advancements and Prospects for Electrocatalytic and Photocatalytic Conversion at Low Temperatures. *Adv. Sci.* **2020,** *7* (23), 2001946.
10. Deng, J.; Lin, S.; Fuller, J.; Iniguez, J.; Xiang, D.; Yang, D.; Chan, G.; Chen, H.; Alexandrova, A.; Liu, C., Ambient methane functionalization initiated by electrochemical oxidation of a vanadium (V)-oxo dimer. *Nature Communications* **2020,** *11* (1), 3686.
11. Kim, R. S.; Surendranath, Y., Electrochemical reoxidation enables continuous methane-to-methanol catalysis with aqueous Pt salts. *ACS Cent. Sci.* **2019,** *5* (7), 1179-1186.
12. Foster, N., Direct catalytic oxidation of methane to methanol - a review. *Appl. Catal.* **1985,** *19* (1), 1-11.
13. Sushkevich, V. L.; Palagin, D.; Ranocchiari, M.; van Bokhoven, J. A., Selective anaerobic oxidation of methane enables direct synthesis of methanol. *Science* **2017,** *356* (6337), 523-527.
14. Gunsalus, N. J.; Koppaka, A.; Park, S. H.; Bischof, S. M.; Hashiguchi, B. G.; Periana, R. A., Homogeneous functionalization of methane. *Chem. Rev.* **2017,** *117* (13), 8521-8573.
15. Ravi, M.; Ranocchiari, M.; van Bokhoven, J. A., The direct catalytic oxidation of methane to methanol-A critical assessment. *Angew. Chem. Int. Ed.* **2017,** *56* (52), 16464-16483.
16. Mahyuddin, M.; Shiota, Y.; Yoshizawa, K., Methane selective oxidation to methanol by metal-exchanged zeolites: a review of active sites and their reactivity. *Catalysis Science & Technology* **2019,** *9* (8), 1744-1768.
17. Andrikopoulos, P.; Michel, C.; Chouzier, S.; Sautet, P., In silico screening of iron-oxo catalysts for CH bond cleavage. *ACS Catal.* **2015,** *5* (4), 2490-2499.
18. Ensing, B.; Buda, F.; Gribnau, M.; Baerends, E., Methane-to-methanol oxidation by the hydrated iron(IV) oxo species in aqueous solution: A combined DFT and car-parrinello molecular dynamics study. *Journal of the American Chemical Society* **2004,** *126* (13), 4355-4365.
19. Szecsenyi, A.; Li, G.; Gascon, J.; Pidko, E., Mechanistic complexity of methane oxidation with H2O2 by single-site Fe/ZSM-5 catalyst. *ACS Catal.* **2018,** *8* (9), 7961-7972.
20. Sirajuddin, S.; Rosenzweig, A. C., Enzymatic oxidation of methane. *Biochemistry* **2015,** *54* (14), 2283-94.
21. Lee, S.; McCormick, M.; Lippard, S.; Cho, U., Control of substrate access to the active site in methane monooxygenase. *Nature* **2013,** *494* (7437), 380-384.
22. Omasta, T. J.; Rigdon, W. A.; Lewis, C. A.; Stanis, R. J.; Liu, R.; Fan, C. Q.; Mustain, W. E., Two pathways for near room temperature electrochemical conversion of methane to methanol. *ECS Transactions* **2015,** *66* (8), 129-136.
23. Spinner, N.; Mustain, W., Electrochemical methane activation and conversion to oxygenates at room temperature. *Journal of the Electrochemical Society* **2013,** *160* (11), F1275-F1281.
24. Spinner, N.; Mustain, W., Influence of non-conducting zirconia on the electrochemical performance of nickel oxide in alkaline media at room temperature. *Journal of the Electrochemical Society* **2012,** *159* (12), E187-E192.
25. Ma, M.; Jin, B. J.; Li, P.; Jung, M. S.; Kim, J. I.; Cho, Y.; Kim, S.; Moon, J. H.; Park, J. H., Ultrahigh electrocatalytic conversion of methane at room temperature. *Adv. Sci.* **2017,** *4* (12), 1700379.
26. Oh, C.; Kim, J.; Hwang, Y. J.; Ma, M.; Park, J. H., Electrocatalytic methane oxidation on Co3O4- incorporated ZrO2 nanotube powder. *Applied Catalysis B-Environmental* **2021,** *283*, 119653.
27. Jang, J.; Rüscher, M.; Winzely, M.; Morales‐Guio, C. G., Gastight rotating cylinder electrode: Toward decoupling mass transport and intrinsic kinetics in electrocatalysis. *AIChE Journal* **2022,** *68* (5), e17605.
28. Song, Y. F.; Zhao, Y. H.; Nan, G. Z.; Chen, W.; Guo, Z. K.; Li, S. G.; Tang, Z. Y.; Wei, W.; Sun, Y. H., Electrocatalytic oxidation of methane to ethanol via NiO/Ni interface. *Applied Catalysis B-Environmental* **2020,** *270*, 118888.
29. Guo, Z.; Chen, W.; Song, Y.; Dong, X.; Li, G.; Wei, W.; Sun, Y., Efficient methane electrocatalytic conversion over a Ni-based hollow fiber electrode. *Chinese Journal of Catalysis* **2020,** *41* (7), 1067-1072.
30. Li, J. L.; Yao, L. B.; Wu, D. Z.; King, J.; Chuang, S. S. C.; Liu, B.; Peng, Z. M., Electrocatalytic methane oxidation to ethanol on iron-nickel hydroxide nanosheets. *Applied Catalysis B-Environmental* **2022,** *316*, 121657.
31. Prajapati, A.; Collins, B. A.; Goodpaster, J. D.; Singh, M. R., Fundamental insight into electrochemical oxidation of methane towards methanol on transition metal oxides. *Proceedings of the National Academy of Sciences* **2021,** *118* (8), e2023233118.
32. Prajapati, A.; Sartape, R.; Kani, N.; Gauthier, J.; Singh, M., Chloride-Promoted High-Rate Ambient Electrooxidation of Methane to Methanol on Patterned Cu-Ti Bimetallic Oxides. *ACS Catal.* **2022,** *12* (22), 14321-14329.
33. Boyd, M.; Latimer, A.; Dickens, C.; Nielander, A.; Hahn, C.; Norskov, J.; Higgins, D.; Jaramillo, T., Electro-

oxidation of methane on platinum under ambient conditions. *ACS Catal.* **2019,** *9* (8), 7578-7587.
34. Morales-Guio, C.; Liardet, L.; Hu, X., Oxidatively electrodeposited thin-film transition metal (oxy)hydroxides as oxygen evolution catalysts. *Journal of the American Chemical Society* **2016,** *138* (28), 8946-8957.
35. Richard, D.; Tom, M.; Jang, J.; Yun, S. G.; Christofides, P. D.; Morales-Guio, C. G., Quantifying transport and electrocatalytic reaction processes in a gastight rotating cylinder electrode reactor via integration of Computational Fluid Dynamics modeling and experiments. *Electrochimica Acta* **2023,** *440*, 141698.
36. Kresse, G.; Hafner, J., Ab initio molecular-dynamics simulation of the liquid-metal-amorphous-semiconductor transition in germanium. *Physical Review B* **1994,** *49* (20), 14251-14269.
37. Kresse, G.; Joubert, D., From ultrasoft pseudopotentials to the projector augmented-wave method. *Physical Review B* **1999,** *59* (3), 1758-1775.
38. Kresse, G.; Furthmuller, J., Efficiency of ab-initio total energy calculations for metals and semiconductors using a plane-wave basis set. *Computational Materials Science* **1996,** *6* (1), 15-50.
39. Kresse, G.; Furthmuller, J., Efficient iterative schemes for ab initio total-energy calculations using a plane-wave basis set. *Physical Review B* **1996,** *54* (16), 11169-11186.
40. Perdew, J.; Burke, K.; Ernzerhof, M., Generalized gradient approximation made simple. *Physical Review Letters* **1996,** *77* (18), 3865-3868.
41. Garcia-Mota, M.; Bajdich, M.; Viswanathan, V.; Vojvodic, A.; Bell, A.; Norskov, J., Importance of Correlation in Determining Electrocatalytic Oxygen Evolution Activity on Cobalt Oxides. *Journal of Physical Chemistry C* **2012,** *116* (39), 21077-21082.
42. Bajdich, M.; Garcia-Mota, M.; Vojvodic, A.; Norskov, J.; Bell, A., Theoretical Investigation of the Activity of Cobalt Oxides for the Electrochemical Oxidation of Water. *Journal of the American Chemical Society* **2013,** *135* (36), 13521-13530.
43. Nurlaela, E.; Wang, H.; Shinagawa, T.; Flanagan, S.; Ould-Chikh, S.; Qureshi, M.; Mics, Z.; Sautet, P.; Le Bahers, T.; Canovas, E.; Bonn, M.; Takanabe, K., Enhanced Kinetics of Hole Transfer and Electrocatalysis during Photocatalytic Oxygen Evolution by Cocatalyst Tuning. *ACS Catal.* **2016,** *6* (7), 4117-4126.
44. Chivot, J.; Mendoza, L.; Mansour, C.; Pauporte, T.; Cassir, M., New insight in the behaviour of Co-H(2)Osystem at 25-150 degrees C, based on revised Pourbaix diagrams. *Corrosion Science* **2008,** *50* (1), 62-69.
45. Curutchet, A.; Colinet, P.; Michel, C.; Steinmann, S.; Le Bahers, T., Two-sites are better than one: revisiting the OER mechanism on CoOOH by DFT with electrode polarization. *Phys. Chem. Chem. Phys.* **2020,** *22* (13), 7031-7038.
46. Kumari, S.; Sautet, P., Highly dispersed Pt atoms and clusters on hydroxylated indium tin oxide: a view from first-principles calculations. *Journal of Materials Chemistry A* **2021,** *9* (28), 15724-15733.
47. Kumari, S.; Masubuchi, T.; White, H. S.; Alexandrova, A.; Anderson, S. L.; Sautet, P., Electrocatalytic hydrogen evolution at full atomic utilization over ITO-supported sub-nano Ptn clusters: High, size-dependent activity controlled by fluxional Pt hydride species. *Journal of the American Chemical Society* **2023**, DOI: 10.1021/jacs.2c13063.
48. Dudarev, S.; Botton, G.; Savrasov, S.; Humphreys, C.; Sutton, A., Electron-energy-loss spectra and the structural stability of nickel oxide: An LSDA+U study. *Physical Review B* **1998,** *57* (3), 1505-1509.
49. Mathew, K.; Sundararaman, R.; Letchworth-Weaver, K.; Arias, T. A.; Hennig, R. G., Implicit solvation model for density-functional study of nanocrystal surfaces and reaction pathways. *J Chem Phys* **2014,** *140* (8), 084106.
50. Mathew, K.; Kolluru, V. S. C.; Mula, S.; Steinmann, S. N.; Hennig, R. G., Implicit self-consistent electrolyte model in plane-wave density-functional theory. *J Chem Phys* **2019,** *151* (23), 234101.
51. Mathew, K.; Kolluru, V. S. C.; Hennig, R. G. VASPsol: Implicit solvation and electrolyte model for density-functional theory. https://github.com/henniggroup/VASPsol (accessed 2023-02-214).
52. Taylor, C.; Wasileski, S.; Filhol, J.; Neurock, M., First principles reaction modeling of the electrochemical interface: Consideration and calculation of a tunable surface potential from atomic and electronic structure. *Physical Review B* **2006,** *73* (16), 165402.
53. Hajar, Y.; Treps, L.; Michel, C.; Baranova, E.; Steinmann, S., Theoretical insight into the origin of the electrochemical promotion of ethylene oxidation on ruthenium oxide. *Catalysis Science & Technology* **2019,** *9* (21), 5915-5926.
54. Kanan, M.; Surendranath, Y.; Nocera, D., Cobalt-phosphate oxygen-evolving compound. *Chemical Society Reviews* **2009,** *38* (1), 109-114.
55. Burke, M. S.; Enman, L. J.; Batchellor, A. S.; Zou, S.; Boettcher, S. W., Oxygen Evolution Reaction Electrocatalysis on Transition Metal Oxides and (Oxy)hydroxides: Activity Trends and Design Principles. *Chemistry of Materials* **2015,** *27* (22), 7549-7558.
56. Lee, B.; Sakamoto, Y.; Hirabayashi, D.; Suzuki, K.; Hibino, T., Direct oxidation of methane to methanol over proton conductor/metal mixed catalysts. *J. Catal.* **2010,** *271* (2), 195-200.
57. Risch, M.; Ringleb, F.; Kohlhoff, M.; Bogdanoff, P.; Chernev, P.; Zaharieva, I.; Dau, H., Water oxidation by amorphous cobalt-based oxides: in situ tracking of redox transitions and mode of catalysis. *Energy & Environmental Science* **2015,** *8* (2), 661-674.
58. Klingan, K.; Ringleb, F.; Zaharieva, I.; Heidkamp, J.; Chernev, P.; Gonzalez-Flores, D.; Risch, M.; Fischer, A.; Dau, H., Water Oxidation by Amorphous Cobalt-Based Oxides: Volume Activity and Proton Transfer to Electrolyte Bases. *Chemsuschem* **2014,** *7* (5), 1301-1310.
59. Fornaciari, J. C.; Primc, D.; Kawashima, K.; Wygant, B. R.; Verma, S.; Spanu, L.; Mullins, C. B.; Bell, A. T.; Weber, A. Z., A Perspective on the Electrochemical Oxidation of Methane to Methanol in Membrane Electrode Assemblies. *ACS Energy Lett.* **2020,** *5* (9), 2954-2963.
60. Stevens, M.; Enman, L.; Korkus, E.; Zaffran, J.; Trang, C.; Asbury, J.; Kast, M.; Toroker, M.; Boettcher, S., Ternary Ni-Co-Fe oxyhydroxide oxygen evolution catalysts: Intrinsic activity trends, electrical conductivity, and electronic band structure. *Nano Research* **2019,** *12* (9), 2288-2295.
61. Morales-Guio, C.; Mayer, M.; Yella, A.; Tilley, S.; Gratzel, M.; Hu, X., An optically transparent iron nickel oxide catalyst for solar water splitting. *Journal of the American Chemical Society* **2015,** *137* (31), 9927-9936.
62. Gerken, J.; McAlpin, J.; Chen, J.; Rigsby, M.; Casey, W.; Britt, R.; Stahl, S., Electrochemical Water Oxidation with Cobalt-Based Electrocatalysts from pH 0-14: The Thermodynamic Basis for Catalyst Structure, Stability, and Activity. *Journal of the American Chemical Society* **2011,** *133* (36), 14431-14442.
63. Gannouni, A.; Delbecq, F.; Zina, M.; Sautet, P., Oxidation of methane to methanol over single site palladium oxide species on silica: A mechanistic view from DFT. *Journal of Physical Chemistry a* **2017,** *121* (29), 5500-5508.
64. Goltl, F.; Michel, C.; Andrikopoulos, P.; Love, A.; Hafner, J.; Hermans, I.; Sautet, P., Computationally exploring

confinement effects in the methane-to-methanol conversion over iron-oxo centers in zeolites. *ACS Catal.* **2016,** *6* (12), 8404-8409.
65. Lee, B.; Hibino, T., Efficient and selective formation of methanol from methane in a fuel cell-type reactor. *J. Catal.* **2011,** *279* (2), 233-240.
66. Tomita, A.; Nakajima, J.; Hibino, T., Direct oxidation of methane to methanol at low temperature and pressure in an electrochemical fuel cell. *Angew. Chem. Int. Ed.* **2008,** *47* (8), 1462-1464.
67. Hibino, T.; Kobayashi, K.; Nagao, M.; Dongwen, Z.; Siyuan, C., Two-stage electrolysis of H2O and CO2 to methanol: CO2-to-methane reduction at the cathode and subsequent methane-to-methanol oxidation at the anode. *Journal of Materials Chemistry a* **2022,** *10* (42), 22718-22729.

TOC Graphic